ADVANCED CONTROL STRATEGIES FOR DIESEL ENGINE THERMAL MANAGEMENT AND CLASS 8 TRUCK PLATOONING

A Thesis

Submitted to the Faculty

of

Purdue University

by

John L. Foster

In Partial Fulfillment of the

Requirements for the Degree

of

Master of Science

August 2020

Purdue University

West Lafayette, Indiana

THE PURDUE UNIVERSITY GRADUATE SCHOOL
STATEMENT OF THESIS APPROVAL

Dr. Gregory M. Shaver, Chair

School of Mechanical Engineering

Dr. Terrence R. Meyer

School of Mechanical Engineering

Dr. John H. Lumkes Jr

School of Agricultural and Biological Engineering

Approved by:

Dr. Nicole L. Key

Head of the School Graduate Program

To Morgan.

ACKNOWLEDGMENTS

This work would not have been possible without significant contributions from a huge group of amazing people, including those who have worked on these projects before me, those who worked alongside me, and those who have helped me through graduate school personally.

Specifically I need to thank:

Dr. Greg Shaver, for bring me on to these projects and providing guidance and motivation for my work.

All the folks at Cummins, Peloton, Eaton, ARPA-E, and JTRP for their support of this work and consistent assistance.

Cody Allen and Dheeraj Gosala, for sparking my interest in the VVA project and being a huge part of why I joined this lab.

Ryan Thayer, for making things happen (and for his incredible patience).

Brady Black, Miles Droege, and Shubham Ashta, for being the best team I've ever been apart of (both the most effective and the most fun) and great friends.

Mrunal Joshi and Kalen Vos, for patiently sharing their knowledge and showing me how to function as a grad student.

Chisom Emegoakor, for his hardworking attitude.

Shveta Dhamankar, for being wicked smart and a considerate friend.

Eric Holloway and Julia Sibley, for keeping all of the work in this thesis organized and on-track.

Jairo Sandoval and James Kuszmaul, for many long phone calls and endless help.

All the folks I've worked with during my internships at Detroit, DTNA, and Cummins (in particular Jeff, Nirmal, Murad, Eli, Alessandro, Ben, and Ana), for putting their trust in me and the incredible amount that I learned from them.

Jim Adelsperger, for being a mentor and consistent advocate.

My parents, my brothers, and my grandparents, for always having my back and being there to support me.

Morgan, for her love and her kindness. God, for carrying me through this.

And everyone else I've had the honor of working with; there's too many of you to list here, but I couldn't have done this without you all.

TABLE OF CONTENTS

Page

LIST OF TABLES

LIST OF FIGURES

Figure Page

ABBREVIATIONS

2SB	2-stroke breathing
AC	alternating current
AFR	air-fuel ratio
aTDC	after top dead center
CAN	controller area network
CARB	California Air Resource Board
CDA	cylinder deactivation
CNG	compressed natural gas
DOC	diesel oxidation catalyst
DPF	diesel particulate filter
DSRC	digital short-range communication
ECM	engine control module
EEVO	early exhaust valve opening
EGR	exhaust gas recirculation
EPA	Environmental Protection Agency
EVC	exhaust valve closing
EVO	exhaust valve opening
GDP	gross domestic product
GHG	greenhouse gas
GPS	global positioning system
GVW	gross vehicle weight
HD-FTP	heavy-duty federal test procedure
IMP	intake manifold pressure
LEVO	late exhaust valve opening
LIVO	late intake valve opening

MPC	model predictive control
MY	model year
NOx	oxides of nitrogen
NVO	negative valve overlap
PECU	platooning electronic control unit
PI	proportional-integral
PID	proportional-integral-derivative
PM	particulate matter
SAE	Society of Automotive Engineers
SCR	selective catalytic reduction
SCRF	selective catalytic reduction filter
SOI	start of injection
TM	thermal management
TOT	turbine outlet temperature
VGT	variable geometry turbocharger
VVA	variable valve actuation

ABSTRACT

Foster, John L. MSME, Purdue University, August 2020. Advanced Control Strategies for Diesel Engine Thermal Management and Class 8 Truck Platooning. Major Professor: Gregory M. Shaver, School of Mechanical Engineering.

Commercial vehicles in the United States account for a significant fraction of greenhouse gas emissions and NOx emissions. The objectives of this work are reduction in commercial vehicle NOx emissions through enhanced aftertreatment thermal management via diesel engine variable valve actuation and the reduction of commercial vehicle fuel consumption/GHG emissions by enabling more effective class 8 truck platooning.

First, a novel diesel engine aftertreatment thermal management strategy is proposed which utilizes a 2-stroke breathing variable value actuation strategy to increase the mass flow rate of exhaust gas. Experiments showed that when allowed to operate with modestly higher engine-out emissions, temperatures comparable to baseline could be achieved with a 1.75x exhaust mass flow rate, which could be beneficial for heating the SCR catalyst in a cold-start scenario.

Second, a methodology is presented for characterizing aerodynamic drag coefficients of platooning trucks using experimental track-test data, which allowed for the development of high-fidelity platoon simulations and thereby enabled rapid development of advanced platoon controllers. Single truck and platoon drag coefficients were calculated for late model year Peterbilt 579's based on experimental data collected during J1321 fuel economy tests for a two-truck platoon at 65 mph with a 55' truck gap. Results show drag coefficients of 0.53, 0.50, and 0.45 for a single truck, a platoon front truck, and a platoon rear truck, respectively.

Finally, a PID-based platoon controller is presented for maximizing fuel savings and gap control on hilly terrain using a dynamically-variable platoon gap. The con-

troller was vetted in simulation and demonstrated on a vehicle in closed-course functionality testing. Simulations show that the controller is capable of 6-9% rear truck fuel savings on a heavily-graded route compared to a production-intent platoon controller, while increasing control over the truck gap to discourage other vehicles from cutting in.

1. INTRODUCTION

1.1 Motivation

Commercial vehicles play a critical role in global infrastructure, enabling the exchange of goods that the world economy depends on. In fact, on-highway trucks in the US transported almost 13 trillion dollars of cargo in 2018 [1], which means that around 57% of the national GDP is moved on trucks at some point. There's no indication that this is going to change anytime soon; Figure 1.1 shows projections that trucks' share of the transportation market will grow over the next 25 years.

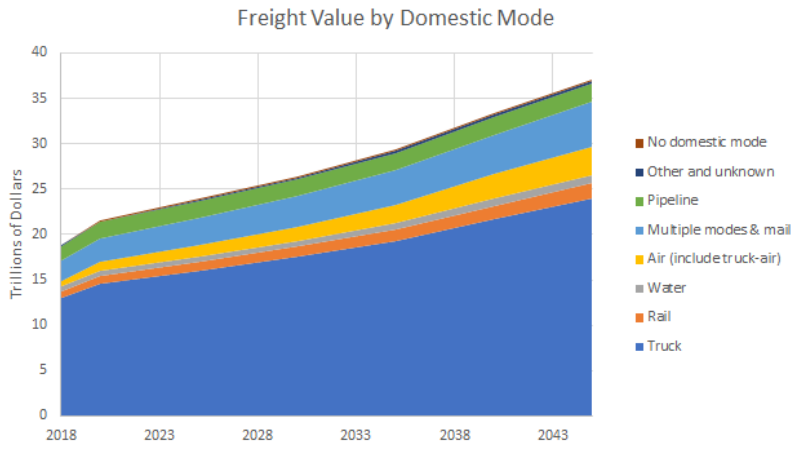

Figure 1.1. Projections of freight value by domestic mode from 2018 to 2045 [1].

Most of these commercial vehicles utilize fossil-fuel-powered combustion engines as their primary form of locomotion. While electrification (with the potential of using a renewable power source) is a growing trend even in the commercial vehicle space, challenges with energy density mean that penetration of electric vehicles into the medium- and heavy-duty markets will be slow (Figure 1.2), and fossil fuel power will dominate the truck market for some time to come [2].

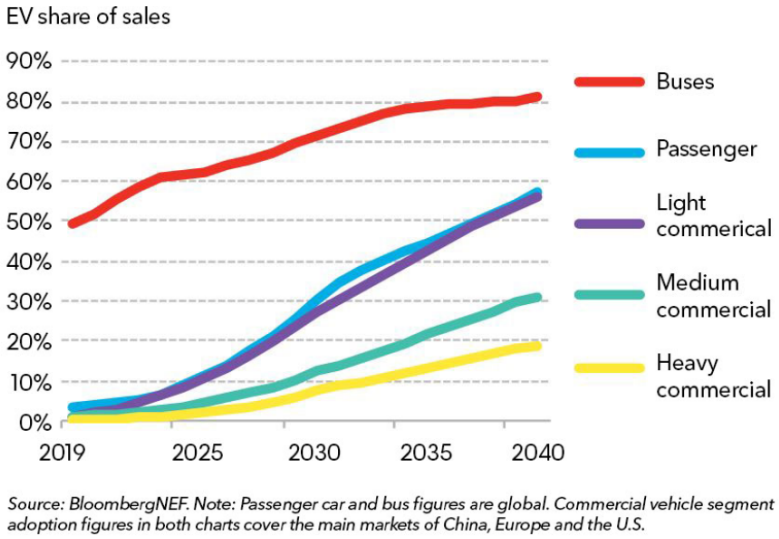

Figure 1.2. Projections for EV share of annual vehicle sales by segment [2].

With every kilogram of fossil fuel burned, greenhouse gases are added to the atmosphere that contribute to global climate change, with transportation as a significant contributor, as shown in Figure 1.3. In 2018, medium- and heavy-duty trucks alone contributed 429 million metric tons of carbon dioxide, 8% of the United States' total [3]. The gigantic scale of the trucking industry manifests in fuel costs as well; estimates are that motor carriers in the US spent 143 billion dollars on fuel in 2015 [4]. Therefore, a perpetual objective of the commercial vehicle industry and of government regulators is the reduction of operating cost and GHG production through the enhancement of vehicle fuel economy. The scale of the problem means that even small changes in vehicle fuel economy could have a profound nation-wide impact, both economically and environmentally.

Oxides of nitrogen (NOx) are another byproduct of fossil fuel combustion. NOx is formed via the chemical reaction known as the Zeldovich mechanism, which takes place during very high temperature combustion. NOx is a major contributer to tropospheric ozone and acid rain, and thus is regulated by the US Environmental Protection Agency (EPA) [5]. Figure 1.4 shows that in the Los Angeles area, where NOx emissions are a significant issue, heavy-duty diesel trucks make up the larges

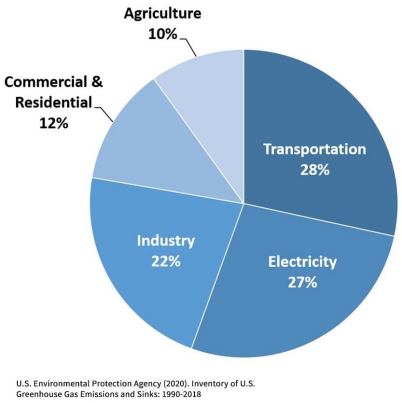

Figure 1.3. Total U.S. greenhouse gas emissions by economic sector in 2018 [3].

share of daily NOx emissions, especially when light- and medium-duty trucks are also included with them. Alternative fuels such as compressed natural gas (CNG) can provide lower NOx emissions, but projections show that diesel will retain market share for some time to come [6], as evident in Figure 1.5. While current diesel technology is able to meet current regulations on NOx emissions, many parts of the country do not meet national air quality standards set forth by the EPA for NOx [7]. In order to improve air quality, significant reductions to the allowable NOx emissions from diesel engines are expected, and novel technological approaches to NOx reduction will be required.

The work that follows in this dissertation aims to advance the collective knowledge base on two particular ideas aimed at tackling these issues: diesel engine aftertreatment thermal management, focused on reducing NOx emissions, and a connected vehicle control strategy called platooning, focused on improving fuel economy.

1.2 Background

1.2.1 Diesel Engine Aftertreatment Thermal Management

There have been regulations on NOx emissions in US since the mid-1980's [9]. Unlike in the passenger car industry, where the vehicle as a whole is certified on a

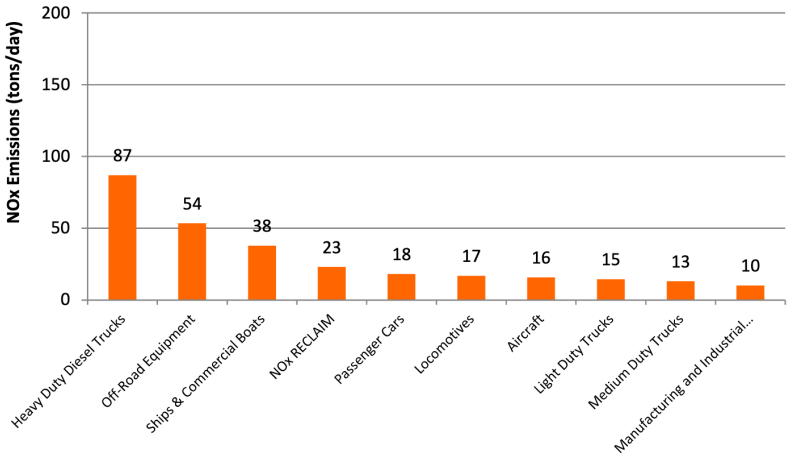

Figure 1.4. Projected daily NOx emissions in Los Angeles by category for Summer 2019 [8].

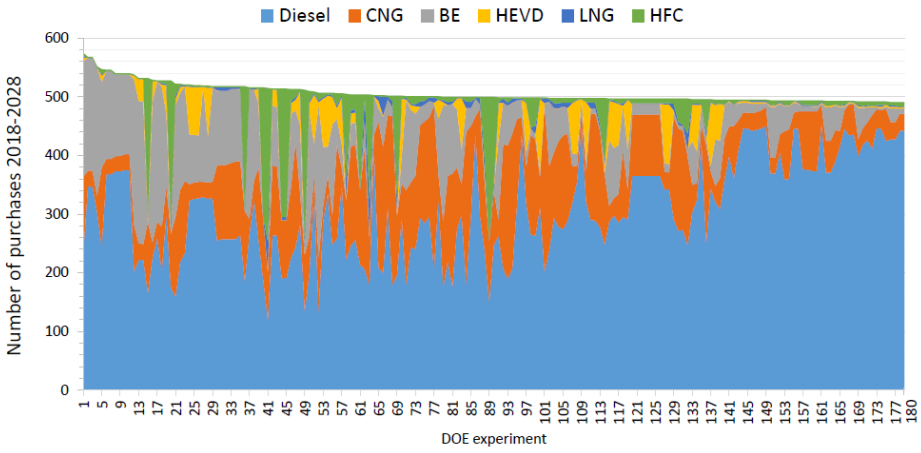

Figure 1.5. Design of experiments projecting powertrain sales through 2028 based on different assumptions of technological readiness level and market conditions [6].

chassis dynamometer, commercial vehicle engines are usually certified on an engine dynamometer, independent of the vehicle, since the same engine is frequently used in many different applications. The applicable certification cycle for on-highway commercial vehicles is the heavy-duty federal test procedure (HD-FTP), a test meant to simulate two 20 minute periods of urban and freeway driving with a 20 minute "hot

soak" in between [10]. Figure 1.6 shows the 20 minute cycle, denoted as a percentage of maximum engine torque and speed so as to be applicable to a variety of engine sizes. The NOx emissions during the drivecycle are measured, weighted, and normalized using the total work done by the engine to get a final NOx emissions number in grams per brake horsepower per hour (g/bhp-hr) [10].

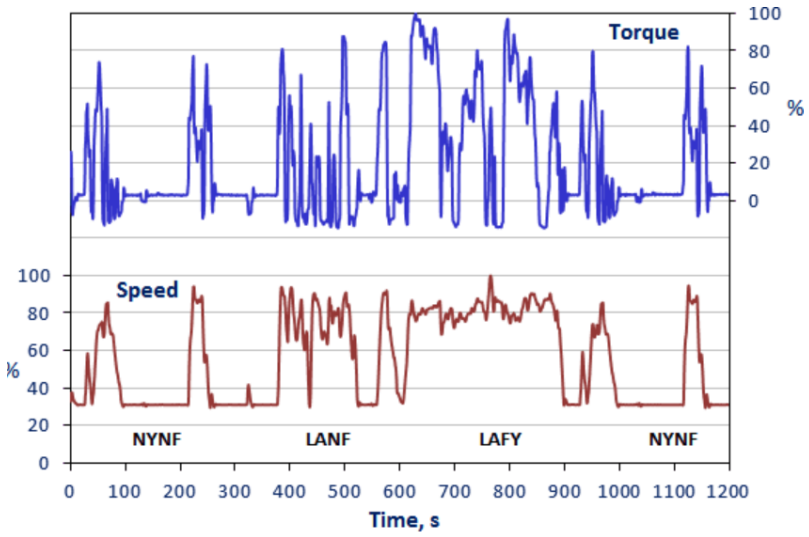

Figure 1.6. Heavy-Duty Federal Test Procedure speed and torque traces as a percentage of maximum [10].

Acceptable HD-FTP NOx limits had been gradually decreasing for years, but the 2007-2010 regulations introduced a drastic drop in the allowable emissions from 2 g/bhp-hr to 0.2 g/bhp-hr, a 90% reduction, sparking a technical renaissance in the commercial vehicle industry as manufacturers worked to meet these new requirements. The strategies most settled on employed a combination of two tactics: reducing the NOx produced through the combustion process, and adding emissions scrubbers to remove NOx from the exhaust before it went out the tailpipe. [11]. The prior relied on exhaust gas recirculation (EGR) for low-NOx combustion, and the latter relied on the urea selective catalytic reduction (SCR), a precious-metal catalytic converter than enables the reaction of NOx with ammonia (injected into the exhaust stream as urea) to form harmless nitrogen gas [12]. Figure 1.7 shows a simplified diagram of

a diesel aftertreatment, which also includes the diesel oxidation catalyst (DOC) and diesel particulate filter (DPF).

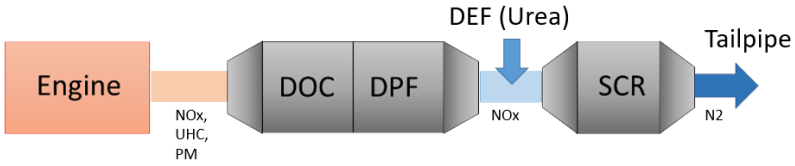

Figure 1.7. Simplified modern aftertreatment system schematic.

However, a key issue with the SCR is its dependence on high temperatures to function effectively. Figure 1.8 demonstrates that while an SCR converts very efficiently at high temperatures, that efficiency drops off significantly below 250°C (the catalyst light-off point). The HD-FTP begins with the engine and aftertreatment system cold, so at the beginning of the first cycle, a high fraction of the NOx produced goes out the tailpipe [13]. This is evident in Figure 1.9, which shows how a substantial fraction of the cumulative cycle tailpipe NOx comes from the first few minutes, before the SCR gets hot enough to convert effectively. Thus, getting the SCR hot as quickly as possible is critical to having low NOx emissions for the cycle as a whole, making it an essential part of the process often referred to as aftertreatment thermal management.

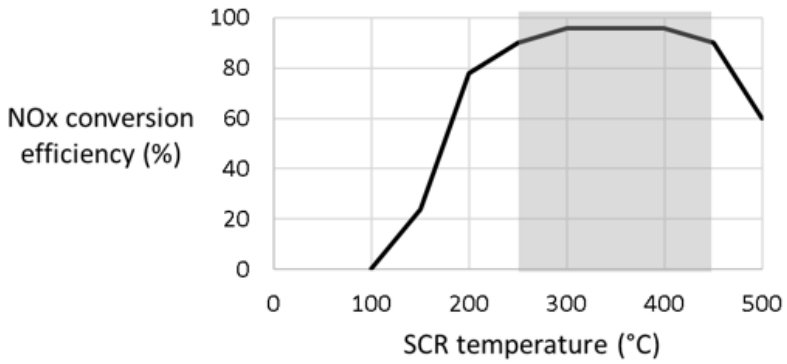

Figure 1.8. SCR NOx conversion efficiency as a function of lumped SCR bed temperature.

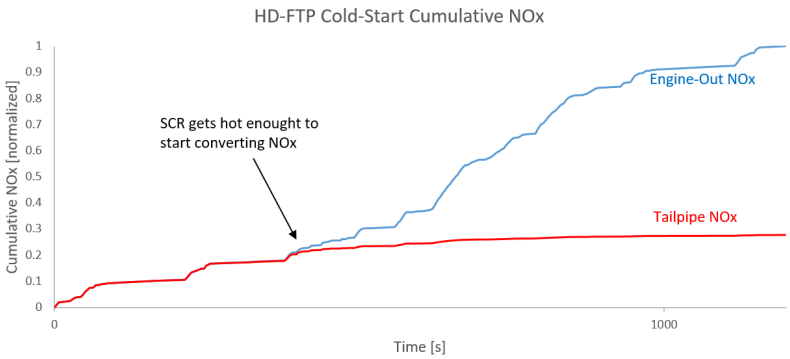

Figure 1.9. Normalized cumulative tailpipe NOx compared to engine-out NOx over the cold-start portion of the HD-FTP.

The state-of-the-art approach to aftertreatment thermal management is centered around increasing the exhaust temperature by making the combustion process less efficient, to increase fuel consumption (and therefore heat) and retain higher temperatures in the exhaust gas after the expansion stroke. Hotter exhaust will travel downstream to the SCR and heat it up more quickly than colder exhaust. Hotter exhaust can be achieved by significantly delaying fuel injections [14] and by closing the variable geometry turbocharger (if one is available). These strategies are shown compared to a more typical fuel economy calibration in Figure 1.10.

These measures are suitable for current regulations, but California Air Resource Board (CARB) has proposed another drastic cut to allow NOx emissions, as much as another 90% reduction, in the 2027 time frame [15]. Meeting such a cut would likely require manufacturers to implement more extreme aftertreatment thermal management measures to heat up the catalyst faster during the critical first minutes of the cycle, including both more aggressive use of existing methods and technologies that are new altogether.

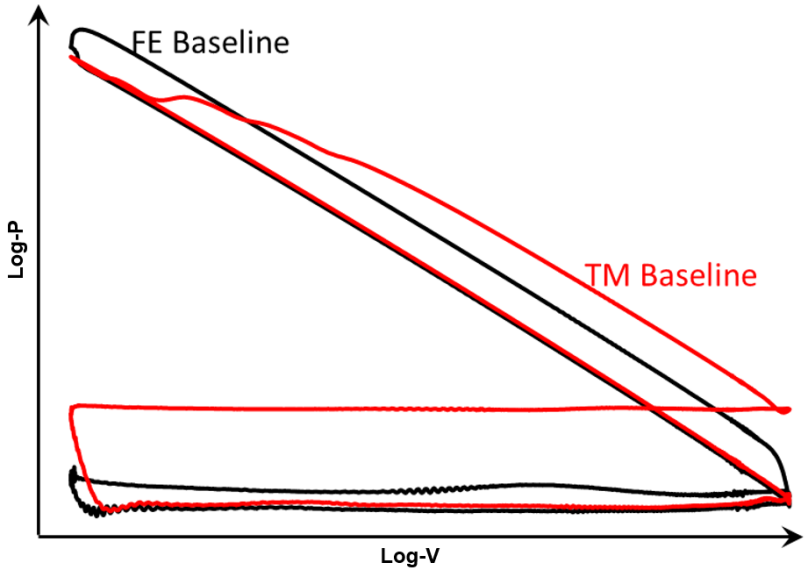

Figure 1.10. Representative PV diagrams for a fuel efficiency calibration and a thermal management calibration.

1.2.2 Class 8 Truck Platooning

Figure 1.11 shows a breakdown of where fuel energy is allocated in a Class 8 truck traveling on level ground at 65 mph, representative of typical operation at highway speeds. When choosing a target for fuel-saving technology, it makes sense to choose an item in the bottom tier, the vehicle-level losses. When the engine is optimized for better efficiency, energy losses are reduced only at the engine level. When the vehicle is optimized for better efficiency, energy losses are reduced at the vehicle level, but additionally the power required from the engine is reduced, so energy losses are reduced at the engine level as well. This essentially makes vehicle-level optimizations doubly effective.

Of the vehicle-level losses, aerodynamics is most dominant [17]. There are several routes to explore for improving tractor-trailer aerodynamics. Tractor aerodynamics hosts many possibilities, including low-clearance air dams, extended fairings, and turning vanes. Replacing side view mirrors with cameras alone could improve aerodynamic efficiency by 5% [18]. Trailer aerodynamics are another opportunity; an EPA

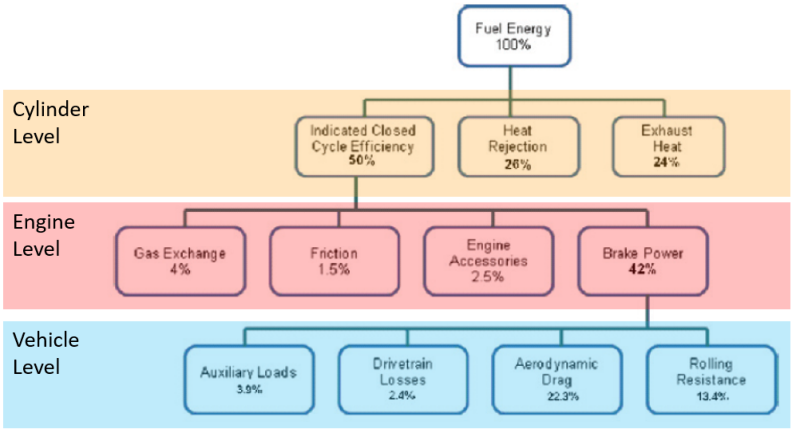

Figure 1.11. Breakdown of energy consumption for a representative class 8 truck at 65 mph on level ground [16].

test demonstrated 9% fuel savings just by modifying trailer aerodynamics [19]. Some have even proposed adding sails to trucks to produce positive thrust [20].

Platooning is another alternative technology that relies on vehicle controls to improve aerodynamics, and may work synergistically with other aerodynamic improvements to a degree. Platooning refers to operating one vehicle very close behind another. As shown in Figure 1.12, this provides a reduction in aerodynamic drag for both trucks, as the front truck breaks the wind for the rear truck and the rear truck reduces the negative pressure region behind the first truck [21]. Generally, the closer the vehicles, the more significant the aerodynamic benefit [22], but close following distances require vehicle-to-vehicle communication to remain safe [21].

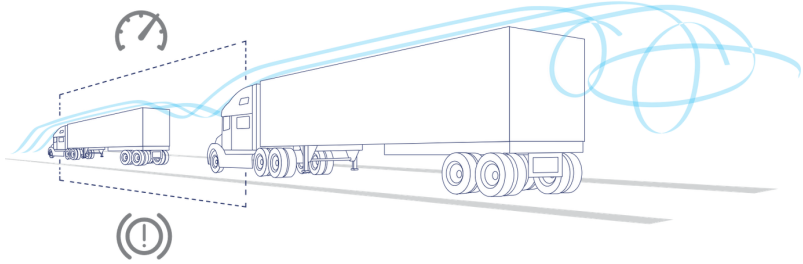

Figure 1.12. Diagram of airflow over two trucks in a platoon [21].

Early-stage real-world trials have already shown combined (averaged between the front and rear trucks) fuel savings of 2.7% for a two-truck platoon [23] and track testing has indicated savings as high as 6.4% should be achievable with modern vehicles [24]. While platooning won't be possible on city streets, in congested traffic, or when there's not another truck nearby, big data analysis of telemetry from about 57,000 class 8 trucks has shown that 56% of vehicle miles traveled would have accommodated platooning [25], giving platooning the potential to have an incredible impact by reducing both fuel costs to operators and GHG emissions.

However, the vast majority of experiments have been performed on relatively flat routes. Platooning on steeply graded routes presents challenges for maintaining the required spacing between vehicles; the maximum possible speed of a heavily-loaded truck decreases on uphill grades, and, in the transition onto the uphill grade, truck spacing can grow significantly [26], which can mitigate the aerodynamic benefits and encourage other vehicles to cut in between the two trucks, breaking the platoon. Figure 1.13 shows a simulation example of this phenomenon, where the rear truck uses the retarder at 16.5 km to maintain the minimum gap when the front truck slows down as it enters the hill, causing it to lose momentum and not be able to keep up with the front truck once it enters the hill.

Additionally, on downhill grades, use of the engine brake/retarder is required to prevent the gap from shrinking [27]. Using the engine brake converts kinetic energy from the vehicle to exhaust heat, which is then wasted and not recoverable. This energy loss ultimately means that more fuel will need to be burned in order to overcome the next hill, increasing vehicle fuel consumption. Figure 1.14 shows a simulation example of this, with the rear truck using the retarder to maintain the minimum gap on the downhill section at 0.8 km.

Both these issues mean that there is meaningful room for improvement for platooning on hilly terrain. Novel platoon controllers that can address these problems, then, could potentially accomplish significant savings.

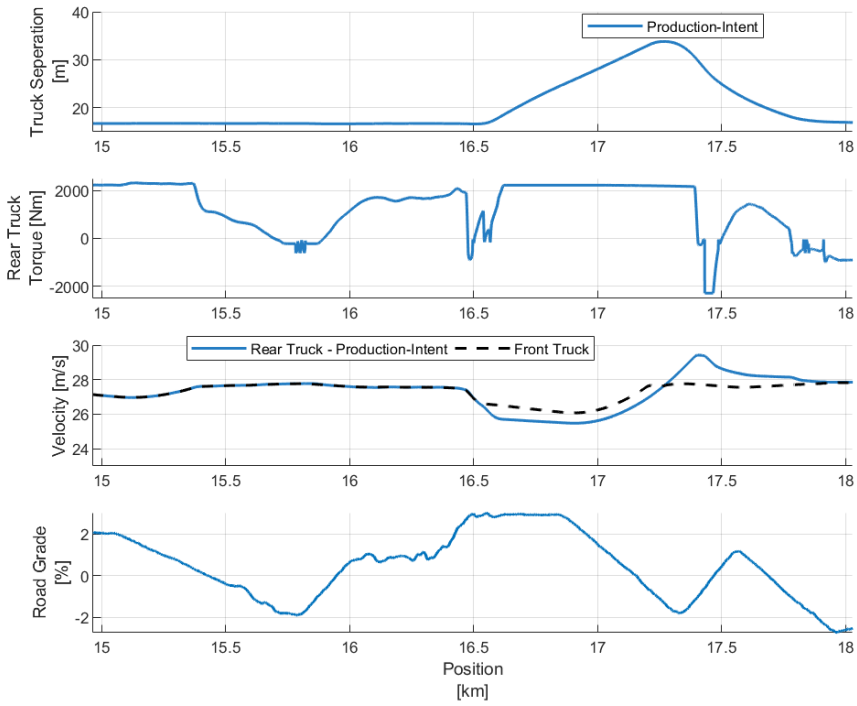

Figure 1.13. Simulated example of gap growth during transitions into steep uphill grades with a production-intent platoon controller.

1.3 Literature Review

1.3.1 Diesel Engine SCR Warm-Up Strategies

As discussed in section 1.2.1, upcoming NOx regulations are expected to drastically cut the amount of permissible NOx emitted over the course of the HD-FTP certification drive cycle. As a significant fraction of the cycle NOx is emitted during the first minutes of the cycle (before the SCR is hot enough to efficiently convert NOx), novel technological approaches to heating the catalyst up more quickly will be critical to meeting the regulations.

Culbertson et al. [28] explored using an electric heating module in the exhaust stream, downstream of the turbine outlet but before the aftertreatment inlet. Using a 30 kW heater, they were able to reach a SCR temperature of 200°C more than 8

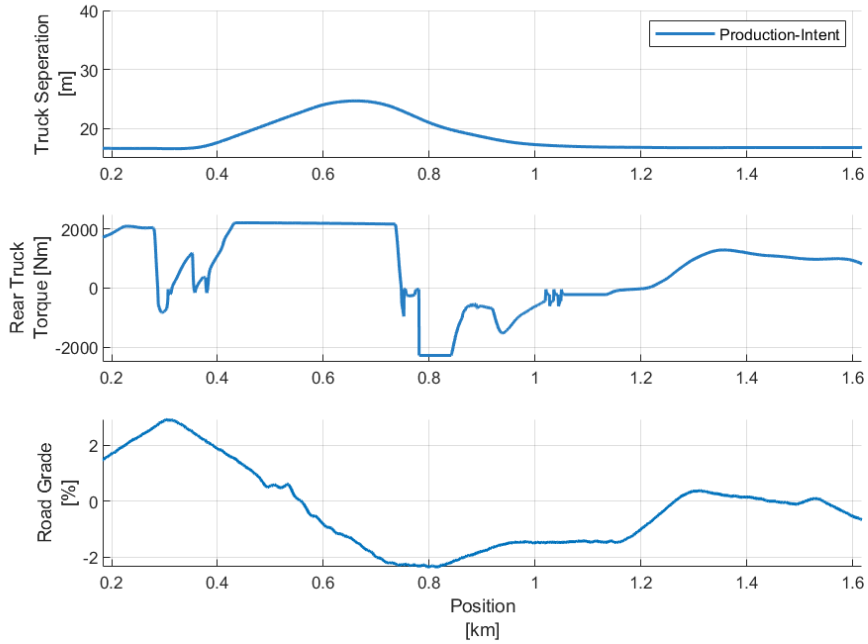

Figure 1.14. Simulated example of rear truck retarder use on downhill grades with a production-intent platoon controller.

minutes earlier into the FTP than without. 30 kw is a significant amount of power, but could be feasible when coupled with a hybrid-electric powertrain, with a larger battery capable of driving the heater. This also raises the possibility of increasing the load on the engine to directly power the heater; this would increase the engine-out exhaust temperature, further helping heat the catalyst.

Another possibility is the integration of a diesel burner into the exhaust stream. A diesel burner, connected to the vehicle fuel supply, could utilize either unburned oxygen in the exhaust stream or siphon air from the intake manifold for combustion, and, in doing so, provide extra heat energy to the SCR, similar to the electric heater. Kimura et al. [29] were able to reduce the time before SCR light-off during the FTP from about 600s to around 100s with such a burner.

Other work has focused on maintaining exhaust temperature between engine outlet and SCR, rather than actively heating the exhaust. While temperature, space,

and chemistry restrictions generally mean that the SCR is placed underfloor in the vehicle, smaller modules with a SCR washcoat applied to a DPF (SCRF) have been developed for placement directly downstream of the turbocharger outlet, to prevent temperature loss between the engine and SCR. When combined with a downstream traditional SCR, an SCRF has been demonstrated to increase steady-state NOx conversion at low temperatures by over 100% and reduce NOx emissions over an FTP72 drive cycle by 50% compared to a traditional SCR [30].

Another way to increase the power transferred from the exhaust gas to the catalyst is by focusing on increasing the mass flow rate of the exhaust rather than the temperature. Vos et al. [31] were able to demonstrate a 51% increase in exhaust mass flow rate at idle (a key operating condition in the FTP) by increasing the engine idle speed from 800 RPM to 1200 RPM, while also seeing an extra 40°C of engine-out temperature.

Work conducted by Southwest Research Institute [32] went further, combining these approaches and adding additional ones, including pre-heated urea dosing, alternate engine calibrations, and passive NOx adsorbers, which can store NOx when the SCR is still cold and release it later. Their work identified several combinations of strategies that could be certified at under 0.02 g/bhp-hr, a 90% reduction from the current regulation.

Variable valve actuation presents more opportunities for faster warm up, with EVO modulation being the most straightforward approach. Gosala et al. [33] used early exhaust valve opening (EEVO) to cut the expansion stroke short, which increases exhaust temperatures considerably both by extracting less energy from the exhaust during the expansion stroke and by increasing the fuel consumption and leading to hotter exhaust. On-engine testing showed exhaust temperatures in excess of 400°C at a steady-state loaded idle condition when coupled with charge trapping via negative valve overlap (EEVC + LIVO), compared to 250°C for a baseline thermal management calibration. Over the FTP, it was predicted to reduce tailpipe NOx by 8%, at the cost of a 7% increase in engine-out PM.

Joshi [34] employed late exhaust valve opening (LEVO), which provided similar benefits to EEVO through recompressing the exhaust gas before exhausting (and thereby increasing the temperature) and by throttling the exhaust valve, both of which require additional fuel consumption, producing higher temperatures. Engine-out exhaust temperatures of almost 350°C where demonstrated without an increase in emissions relative to baseline.

There are many other uses of VVA for aftertreatment thermal management, including, most notably, cylinder deactivation (CDA). However, while CDA is beneficial for stay-warm operation, a defining characteristic of the strategy is low exhaust flow rates. Combining this with exhaust temperatures that don't exceed that of a conventional thermal management strategy means that CDA is not appropriate for warm-up operation [35].

1.3.2 Class 8 Platooning Gap Maintenance Strategies

As discussed in section 1.2.2, while platooning technology is relatively close to market, challenges still remain with controlling the gap and eliminating retarder usage on hilly terrain.

Ibitayo [36] suggested that by coordinating shift events such that the rear truck shifts simultaneously with the front truck, gap maintenance issues on uphill grades could largely be avoided. Simulations showed that this tactic could reduce maximum deviation from a fixed gap setpoint from 18m to 3m on a route with up to 5% grades. This strategy could be relatively simple to implement and doesn't require look-ahead data. However, this analysis was only performed with identical trucks; the effectiveness could vary based on available gear ratios and engine calibrations. Additionally, while synchronized shifting helps minimize gap deviations on uphill grades, it doesn't help prevent retarder usage on downhill grades.

Another approach involves using a simple rule-based controller. Alam et al. (2015) [27] proposed a time-delay controller, where the rear truck follows a version of the

front truck's speed that has been delayed by some time offset, such that the two vehicles achieve the same velocities at the same points in space. This allows the gap to grow before a downhill section (because the front truck speeds up before the rear truck), meaning that less retarder needs to be used to maintain the minimum required gap distance. Simulations showed a reduction in total energy consumption of 9% over a sample route for the rear truck compared to a traditional controller. However, these simulations were performed with a low-fidelity model, and effects on uphill gap control were not demonstrated.

Traditional platoon controllers seek to maintain a constant gap distance. However, the success of the time delay controller hints at the benefits of an alternative methodology. Under certain circumstances, letting the truck spacing grow or shrink can be beneficial for keeping the spacing within the desired range on uphill grades and reducing retarder usage on downhill grades.

A model predictive control (MPC) algorithm can be used for this; it can employ vehicle parameters and look-ahead route data to predict the optimal spacing (or, equivalently, relative speeds) between the trucks at different points on a route, maximizing efficiency while maintaining safety and driver comfort. Such a variable gap MPC optimizer was implemented in simulation by Alam et al. (2013) [37], who predicted fuel savings of 4-14% averaged between both trucks for a simple downhill grade when coupled with look-ahead front truck control (compared to a traditional platoon). While a single downhill grade isn't representative of any realistic route, the study serves as a significant proof of concept.

While allowing the gap to vary may seem counter intuitive when trying to eliminate gap deviation, Ibitayo [36] had success on a heavily-graded route with a similar MPC optimizer by allowing gap to vary only from 16.7m to 25m, compared to deviations all the way out to 35m using a traditional controller with a 16.7m setpoint. In addition, the simulation showed a combined fuel savings of 3% compared to the baseline platoon controller over the same real-world route.

1.4 Contributions

1.4.1 Diesel Engine Variable Valve Actuation

Diesel Engine 2-Stroke Breathing

The author led aftertreatment simulations to motivate 2-stroke breathing by estimating the potential warm-up benefits, co-led the implementation of 2-stroke valve profiles on the testbed with Kalen Vos, co-led screening and data collection with Kalen Vos and Mrunal Joshi, and led the analysis of the resulting data. This effort is detailed in Chapter 3.

Natural Gas Fuel Supply for a VVA Test Cell

The author developed several detailed proposals for installing a natural gas fuel system in the VVA test cell for use in future research projects, created a initial budget estimate for the proposals, and assisted in the process of ordering components for the project, laying the groundwork for a summer 2020 installation. This effort is not detailed in this thesis.

1.4.2 NEXTCAR

Development of a Variable Gap Platoon Controller

The author co-led development of a variable gap platoon controller in simulation with Miles Droege, led the implementation of the controller on the truck, and led the calibration of the controller in closed-track vehicle testing. This effort is detailed in Chapter 5.

Uvalde Functionality Testing

The author assisted in analysis of cruise controller data and functionality testing of a predictive cruise controller with Brady Black, Miles Droege, and Shubham Ashta. This testing and analysis paved the way for the I-69 single truck testing in Indiana. This effort is not detailed in this thesis.

Platoon Aerodynamic Analysis

The author led the development of a methodology from determining drag coefficient of platooning vehicles from experimental testing. This effort is detailed in Chapter 4. The author also led a J2263 coastdown test on a single truck, which is not detailed in this thesis.

I-69 Single Truck Testing

The author co-led single truck testing on I-69 in Indiana with Brady Black, Miles Droege, and Ryan Thayer and co-led updates to vehicle models based on the results with Brady Black and Miles Droege. This testing and analysis prepared the team for eventual platoon fuel economy testing on I-69. This effort is not detailed in this thesis.

1.5 Thesis Outline

Chapter 1 discusses the motivation for diesel engine aftertreatment thermal management and platooning, provides background on the same, and provides a review of literature on both topics.

Chapter 2 provides background on the research testbeds used for the various experiments discussed in this thesis.

Chapter 3 presents motivation, methodology, and results for a novel diesel engine aftertreatment thermal management strategy, including both results constrained to nominal engine emissions and results with more flexible constraints.

Chapter 4 details a novel methodology for experimentally determining drag coefficients for platooning vehicles and presents results of said analysis, as well as single-truck coastdown test results for model validation.

Chapter 5 presents a design for a variable gap platoon controller for a class 8 truck, as well as analysis of the controller's experimental tracking and simulated fuel economy performance.

Chapter 6 provides a summary of the thesis, as well as recommendations for future efforts.

2. EXPERIMENTAL SETUP

2.1 Diesel Engine Test Cell

This section describes the diesel engine testbed utilized for the experiments discussed in Chapter 3. Figure 2.1 shows a schematic of the test cell. The key elements are the Cummins diesel engine, custom hydraulic variable valve actuation (VVA) system, and Powertest AC dynamometer.

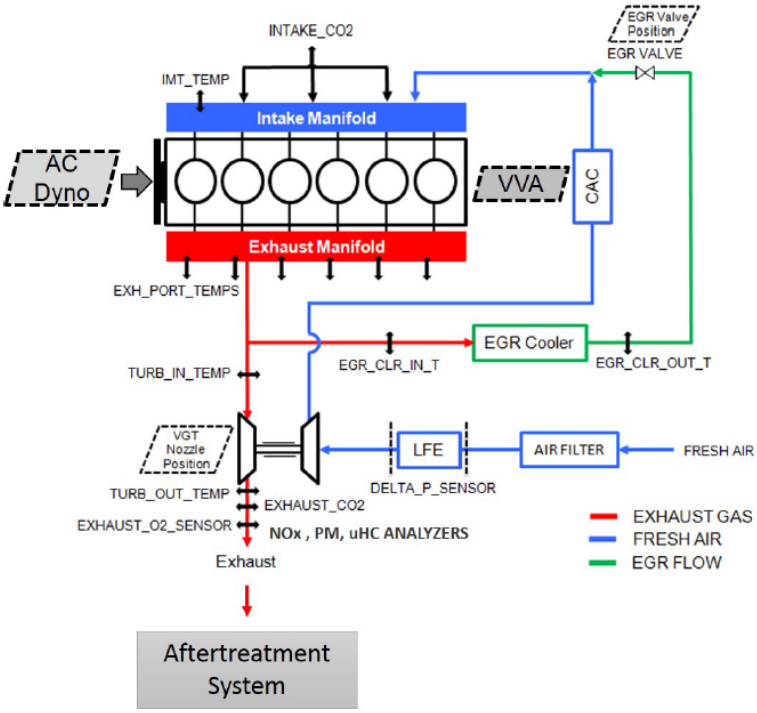

Figure 2.1. Schematic of the diesel engine test cell.

The engine is an inline 6-cylinder diesel engine with a high-presure common rail direct fuel injection system, a split exhaust manifold with high-pressure exhaust gas recirculation and a air-to-coolant EGR cooler, and a nozzle-style variable geometry

turbocharger. Control of all these stock engine actuators is available through a generic serial interface link to the engine control module (ECM). Charge air is aftercooled by a temperature-regulated air-to-water heat exchanger.

The dyno can provide up to 670 hp, and is able to command engine throttle position, giving it ability to control both speed and torque and enabling both motoring and transient operation.

The VVA system features individual intake and exhaust actuators on each cylinder, providing both cylinder-to-cylinder and cycle-to-cycle control of valve timing and lift. The valve timing is coordinated to the engine via a AVL 365C crankshaft encoder. The valves are controlled with a custom-built dSpace program, which uses position feedback via linear variable differential transformers. A schematic of the VVA is shown in Figure 2.2.

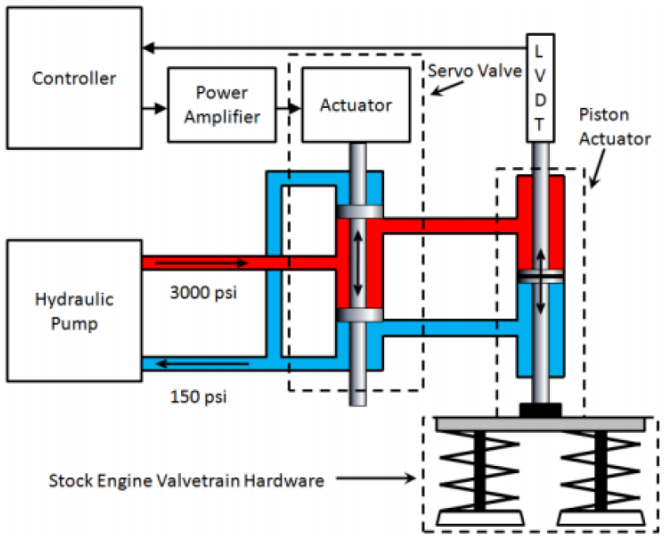

Figure 2.2. Electro-hydraulic variable valve actuation system.

Pressure measurements are logged in all six cylinders using either Kistler 6067C or AVL QC34C pressure transducers and an AVL 621 Indicom module. Fuel injector currents are also measured to verify fuel injection strategies.

NOx is measured at the turbine outlet via the production engine NOx sensor and soot is measured with an AVL 483 MicroSoot meter. Other measurements include Intake/Exhaust CO2 (Cambustion NDIR 500 series analyzers, used to calculate EGR fraction), fresh air flow (laminar flow element), and fuel consumption (Cybermetrix Cyrius gravimetric fuel meter).

2.2 Class 8 Trucks

This section describes the class 8 truck testbeds utilized for the vehicle testing discussed in Chapter 4 and 5.

The trucks themselves are MY2019 Peterbilt Model 579 80" sleeper cabs. They are equipped with modern aerodynamics equipment (steer wheel closeouts, low-clearance air dam, side skirts, side extenders, roof deflector) and safety equipment (audible lane-keeping alerts, adaptive cruise control, blind spot detection). Both are powered by a Cummins X15 efficiency series 15L diesel engine and the integrated Eaton Endurant 12 speed automated manual transmission.

The trailers are 53' Wabash National DuraPlate dry van trailers with trailer skirts. Each tractor-trailer combination is loaded down with concrete blocks to 65,000lb GVW. The tractors with trailers are shown in Figure 2.3.

Both trucks are equipped with the Peloton PlatoonPro platooning system, including the platooning electronic control unit (PECU), driver controls, camera, and display. The platooning system is integrated into the vehicle's controller area network (CAN), which enables it to read data from the vehicle, engine, transmission, and brake module and to command parameters like engine torque during a platoon. The PECU also has its own internal GPS and a digital short-range communication (DSRC) antenna, which allows it to communicate with the PECU in the other truck. The PECU also serves for logging data, relaying it through an LTE connection to a host server.

Figure 2.3. The two identical Peterbilt 579's used for vehicle testing.

For measurement of fuel consumption, a ReiCon TI 6000 Uniflowmaster volumetric flow meter was installed in-line on the fuel system of both trucks. To convert volume to mass, fuel temperature and density measurements are made at the start of each test. Fuel measurements from the ReiCon are collected and logged via the PlatoonPro system.

Speedgoat rapid prototype computers were also installed, enabling the implementation of custom Simulink algorithms. The Speedgoats are equipped with their own separate GPS's, and are able to communicate both over CAN and through separate connections to the engine and PECU, giving them the ability to command engine torque, retarder torque, cruise control setpoint, and transmission gear number. The full vehicle network is laid out in Figure 2.4.

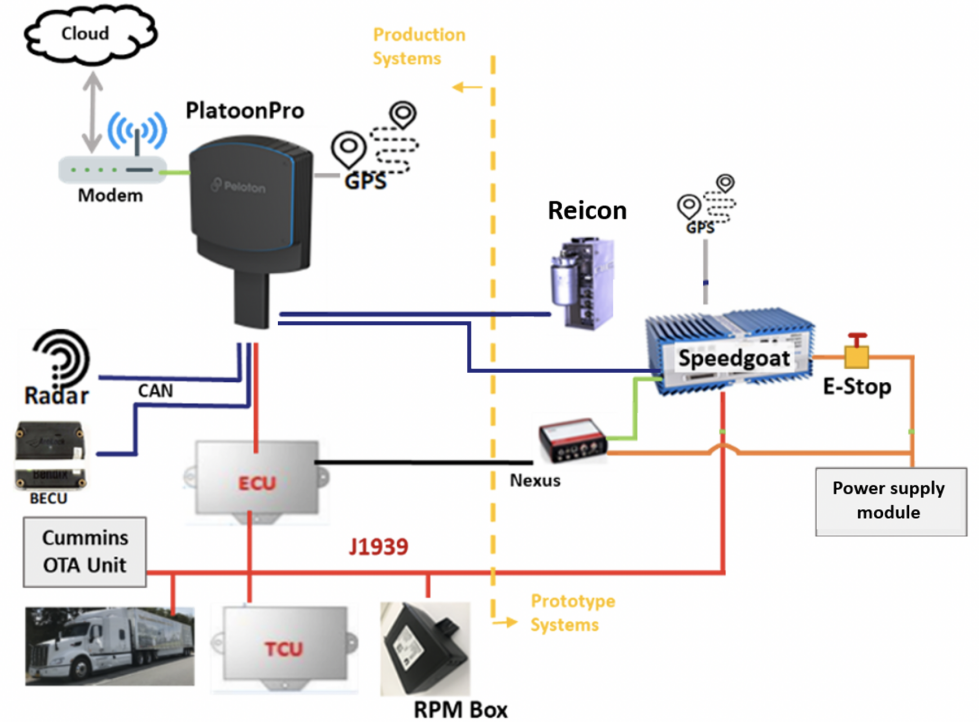

Figure 2.4. Full vehicle control network schematic, with red lines representing the vehicle CAN and blue lines representing Ethernet connections.

3. DIESEL 2-STROKE BREATHING FOR GET-HOT PERFORMANCE

3.1 Motivation

As discussed in section 1.2.1, a key step towards meeting forthcoming NOx emissions regulations is the reduction in the time it takes the SCR to get-hot after a cold start. As presented in section 1.3.1, there are a number of technological possibilities, including advanced aftertreatment hardware, exhaust burners and heaters, and EVO modulation via VVA. Most of these ideas focus on creating or retaining higher temperatures in the exhaust. However, an equally important part of a high heat transfer rate to the catalyst is the mass flow rate of the exhaust gas. The following presents a methodology for achieving high exhaust mass flow rates using VVA, which serves as another possibility for faster SCR warm up.

In a 4-stroke engine (such as is used for these experiments), each cylinder intakes and exhausts its own displacement volume once every two crankshaft rotations. The only ways to increase the mass flow rate under normal conditions are to increase the angular speed of the engine or to increase the density of the air during the intake stroke, perhaps through increased turbocharger boosting or charge cooling. If VVA is present on the engine, however, the engine is not necessarily limited to operating its valves in a traditional 4-stroke cycle.

In 2-stroke breathing (2SB), the strategy detailed here, 3 out of 6 cylinders operate in a conventional 4-stroke cycle and the other 3 cylinders cut out fuel injection and add additional intake and exhaust valve events, similar to the operation of a 2-stroke engine. This strategy was first proposed by Odstrcil [38], who ran GT-Power simulations that indicated a significant exhaust mass flow rate benefit was possible. This work demonstrates 2-stroke breathing implemented on an experimental testbed for the first time.

The operating condition selected for these experiments and analysis was steady-state curb idle, 800 RPM and 1.3 bar BMEP. This operating condition was chosen both for its relevance to the HT-FTP (highlighted in Figure 3.1) and for ease of calibration. Almost 40% of the FTP cycle is at idle, with idle portions concentrated towards the critical first few minutes. Additionally, idle is a significant real-world operating condition; a 2015 NTEA study reported that 66% of commercial vehicles are idled more than 1 hour a day, with 33% being idled more than 3 hours a day [39]. Thus, better thermal management at idle can make a difference both in meeting higher certification emissions limits and in real-world operation.

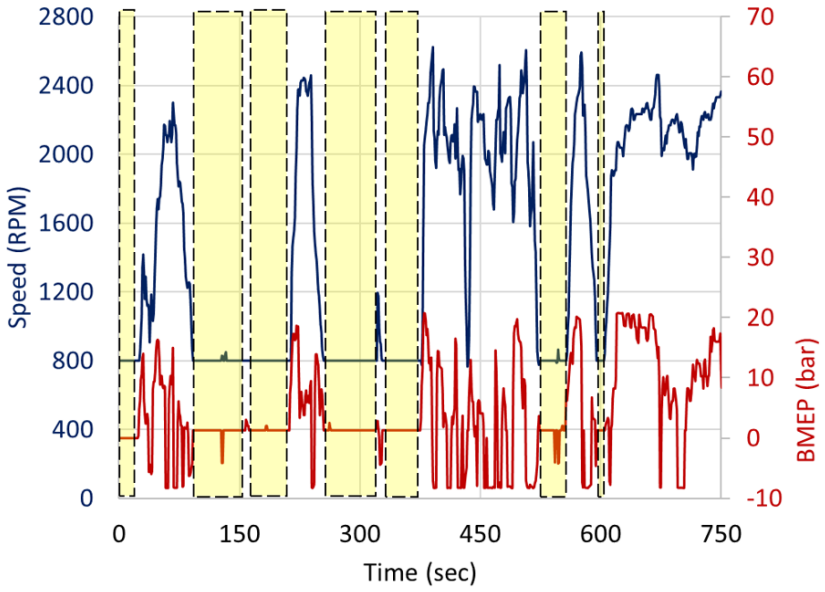

Figure 3.1. HD-FTP test cycle, with idle sections highlighted.

3.2 Strategy Overview

A diagram of 2-stroke breathing operation is shown in Figure 3.2. Cylinders 4, 5, and 6 are operating with a conventional 4-stroke cycle and are producing power for the whole engine. In cylinders 1, 2, and 3, no fuel is being injected, and thus there is no combustion. Instead, extra intake and exhaust valve profiles are added, making

those cylinders pump gas at twice the normal rate, increasing the mass flow rate. An example set of valve profiles for the non-firing cylinders is shown in Figure 3.3. Essentially, the compression and expansion strokes are replaced with additional exhaust and intake strokes, respectively. Note that cylinders 4, 5, and 6 are chosen to be the firing cylinders because the engine has a split exhaust manifold; if cylinders 1, 2, and 3 were firing, fresh air would circulate through the EGR system, making emissions control difficult.

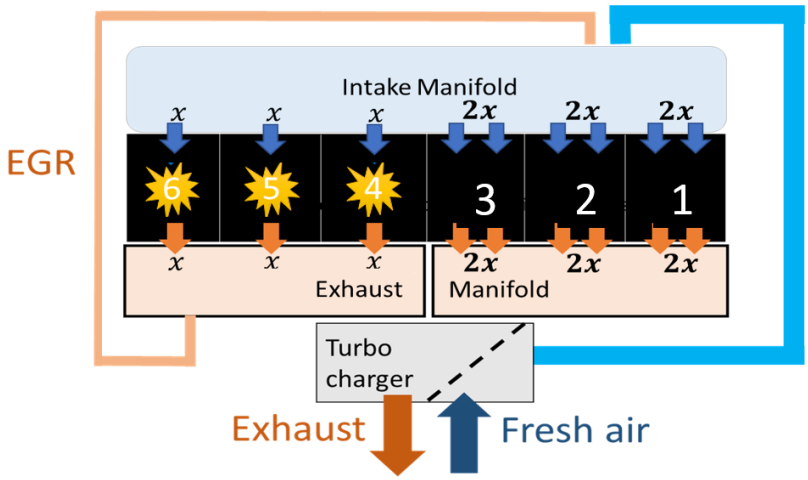

Figure 3.2. Schematic of engine operating with 2-stroke breathing.

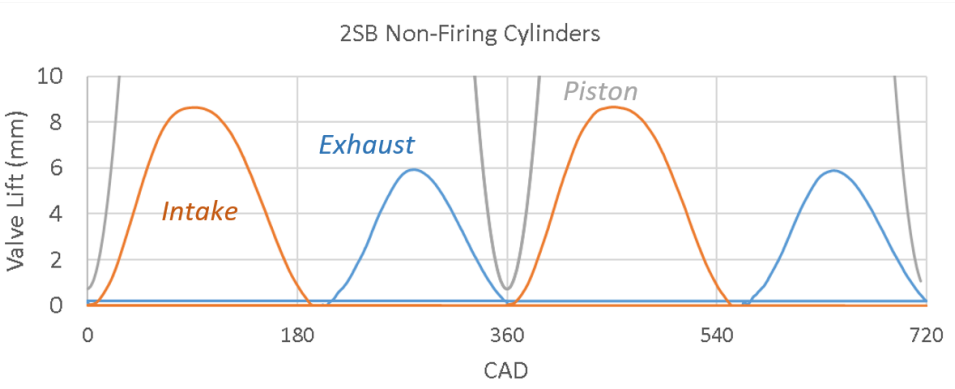

Figure 3.3. Example valve profiles used in 2SB for the non-firing cylinders.

While the non-firing cylinders serve to significantly increase the exhaust mass flow rate, this comes at a temperature penalty. As no combustion is taking place in these cylinders, the gas exhausted from them is relatively cold, which is detrimental to the objective of faster SCR warm up. Therefore, other thermal management measures are also need to be utilized in order to get the exhaust as hot as possible.

3.3 Emissions-Constrained Strategies

The first strategy detailed here is emissions-constrained 2-stroke breathing (labeled "2SB"). At a high level, it follows the procedure described in Section 3.2. The term "emissions-constrained" indicates that it has engine-out NOx and particulate matter (PM) emissions that are less than or equal to those of the engine's stock thermal management calibration (labeled "TM"). This criteria helps ensure that the playing field is level when comparing different strategies. If, for example, a hypothetical strategy produces a higher temperature and mass flow rate than TM but also produces more steady-state NOx, it could reach high SCR temperatures faster but still produce more cumulative tailpipe NOx, as the NOx flow rate would be higher during the periods where the SCR was cold. Therefore, constraining engine-out emissions to those of TM helps provide a fair comparison.

Figure 3.4 a) shows the valve profiles utilized for the 2SB strategy. In the non-firing cylinders, an extra pair of valve profiles is added. The intake valve uses the stock engine valve profiles (just twice as frequently) in order to maximize volumetric efficiency and thereby the mass flow rate of gas. The exhaust valve profiles in the non-firing cylinders are somewhat modified: EVO is delayed in order to prevent significant overlap with the intake strokes, which would create some backflow from the exhaust manifold to the intake manifold, to the detriment of overall mass flow rate. As the valve ramp rates are kept constant, the valve lift shrinks from 8.5mm to 6mm when EVO is delayed.

The initial hope was to leave the valve profiles of the firing cylinders in their OEM configuration. However, during initial screening, difficulty was encountered with a lack of control authority over the EGR valve. Control over EGR is critical, as EGR helps balance NOx and PM emissions against each other. In this case, a mostly-closed EGR valve coupled with an elevated exhaust manifold pressure (due to the high mass flow rate) led to the smallest increment available in EGR valve position being the difference between too much NOx and too much PM. To combat this, internal EGR via negative valve overlap (NVO) was employed by advancing the EVC timing, as shown in Figure 3.4 b). This traps some exhaust gas in the cylinder, functioning as EGR to help control NOx. The EVC position can be more finely adjusted than the EGR valve position, enabling additional control over the EGR fraction.

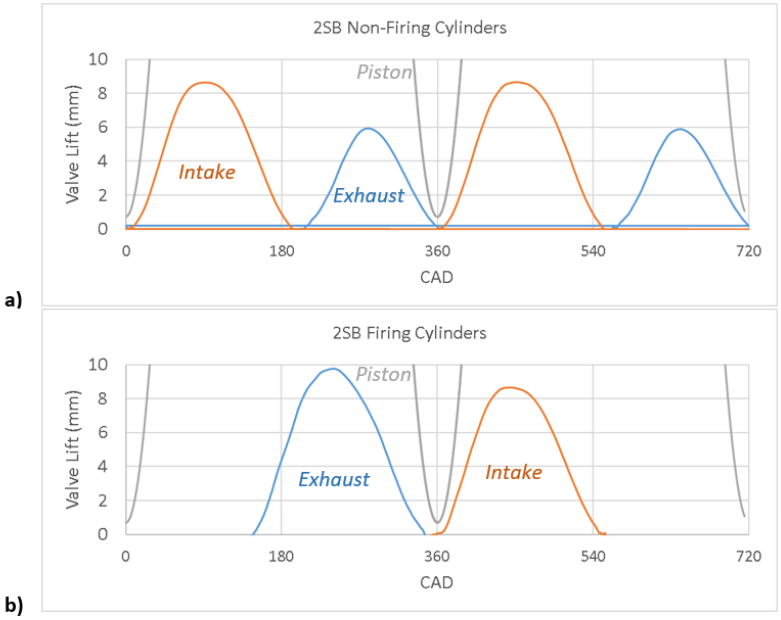

Figure 3.4. Valve profiles utilized in emissions-constrained 2SB for: a) non-firing cylinders and b) firing cylinders.

Figure 3.5 shows the calculated heat release and measured fuel injector currents for TM and the firing cylinders in 2SB, demonstrating the fuel injection strategies. Several of the key methodologies for TM are apparent: start-of-injection (SOI) for

the main injection is retarded to 10° aTDC, and two post injections are used for high exhaust gas temperature. By comparison, 2SB uses an identical SOI, but the first post injection has been advanced and the second post injection has been removed. Note that the comparative length of injection events does not correspond to difference in amount of fuel injected, as the fuel rail pressure for the 2SB case is significantly higher to further help control PM emissions. The higher rail pressure also leads to increased fuel atomization, making the heat release for the 2SB case much faster.

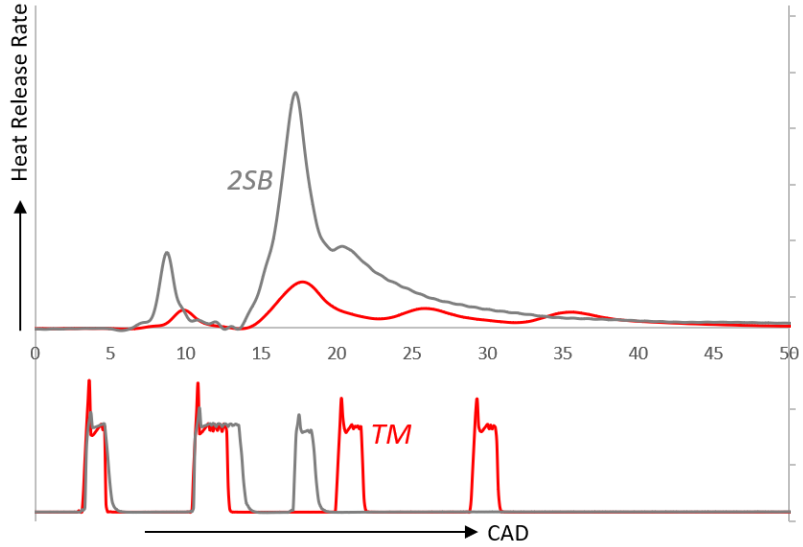

Figure 3.5. Heat release and fuel injector current for firing cylinders in emissions-constrained 2SB, compared to TM calibration.

Figure 3.6 shows the PV plot for TM and the firing cylinders of 2SB. Both strategies utilize a squeezed VGT, which creates backpressure, causing the large pumping loops. This helps increase fuel consumption and drive higher exhaust temperatures. Also apparent is the NVO in the pumping loop of 2SB; the pressure increases when charge is trapped at the end of the exhaust stroke by the valve closing early.

The PV diagram for the non-firing 2SB cylinders is shown in Figure 3.7. It is subject to the same intake and exhaust pressures as the firing cylinders, so it has the same large pumping loop, just without the NVO charge trapping. Note that there are

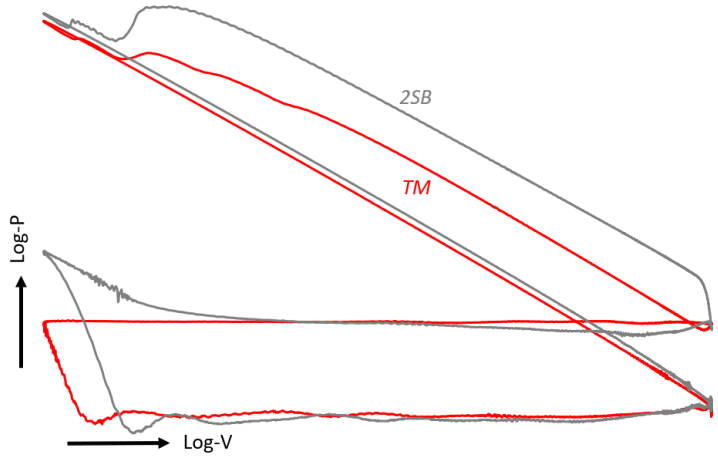

Figure 3.6. PV diagram for firing cylinders in emissions-constrained 2SB, compared to TM calibration.

still two distinct loops, they just fall directly atop each other, as intake and exhaust profiles are identical between the two cycles.

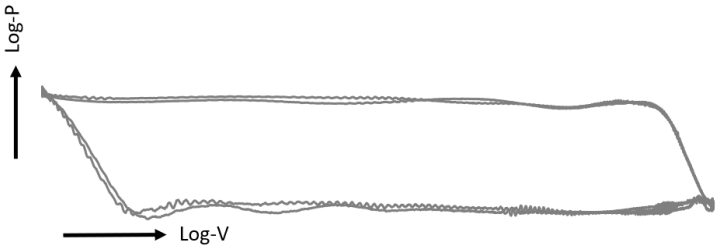

Figure 3.7. PV diagram for non-firing cylinders in emissions-constrained 2SB.

3.4 Flexible-Constraint Strategies

While emissions constraints can be a valuable tool for providing fair points of comparison, emissions-constrained data doesn't necessarily demonstrate a strategy's full capability. There could be cases where engine-out NOx or PM maybe be a secondary

consideration compared to aftertreatment thermal management. For example, engine designers may be willing to accept elevated DPF soot loading for a short period if it means the SCR gets hot faster. Likewise, if a passive NOx adsorber is present, elevated engine-out NOx may be acceptable in exchange for earlier SCR conversion. Additionally, constraints on steady-state emissions don't capture all the dynamics of a cold start; while a high-emissions thermal management strategy increases the rate of emissions production, it could also decrease the time taken for the SCR to heat up. Less time to warm up would mean less time spent in the high-emissions state, possibly allowing cumulative emissions to even be reduced compared to baseline.

For these reasons, 2-stroke breathing strategies that didn't meet rigid emissions constraints were also considered, in order to demonstrate some range of possibility. To provide a fair comparison, thermal management strategies with flexible constraints were developed both using the stock engine actuators (labeled "TM, flexible constraints") and with the addition of 2-stroke breathing (labeled "2SB, flexible constraints").

Figure 3.8 shows the valve profiles developed for the flexible-constraint 2SB case. The non-firing cylinders use identical valve profiles to the emissions-constrained case. The firing cylinders' valves utilize the stock valve profiles, unlike the emissions-constrained case, which utilized NVO for charge trapping. NVO was eliminated to increase simplicity of the strategy, as it was primarily used for emissions control before.

Figure 3.9 shows the measured injector currents and calculated heat releases for the firing cylinders in all four strategies. Note that flexible-constraints 2SB does not use post injections, in contrast to the emissions-constrained case. The flexible-constraint TM strategy has the same injection events as constrained TM, but with more fuel pushed to the post injections instead of the main injection, to help create higher temperatures. The flexible-constraint 2SB strategy uses an elevated fuel rail pressure (though not to the extent of its emissions-constrained counterpart), while the flexible-constraint TM uses a similar rail pressure to constrained TM.

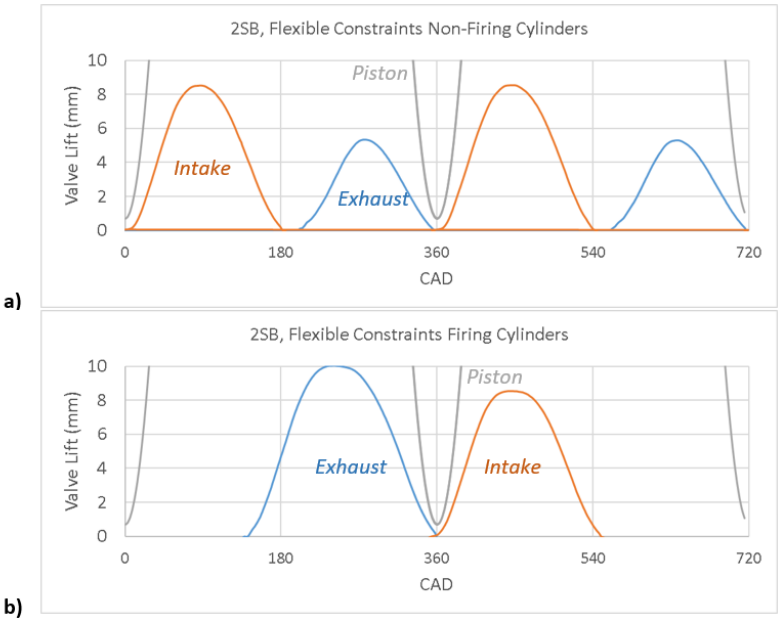

Figure 3.8. Valve profiles utilized in flexible-constraint 2SB for: a) non-firing cylinders and b) firing cylinders.

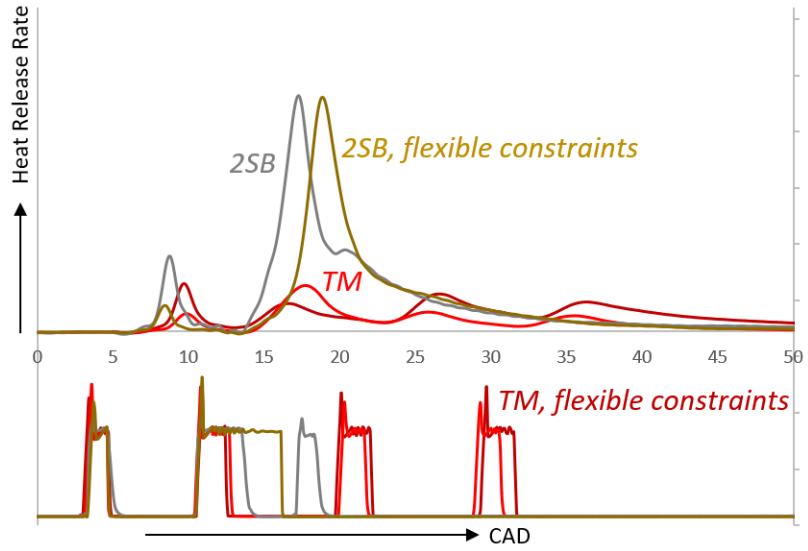

Figure 3.9. Heat release and fuel injector current for firing cylinders in flexible-constraint 2SB and flexible-constraint TM, compared to stock TM calibration.

Figure 3.10 shows the PV diagram for the firing cylinders of both flexible-constraint strategies compared to that of the baseline. Both strategies employ a VGT that is further squeezed shut compared to TM, resulting in a higher exhaust pressure that leads to more pumping work and therefore increased fuel consumption. In the case of flexible-constraint TM, the VGT is in its 100% closed position.

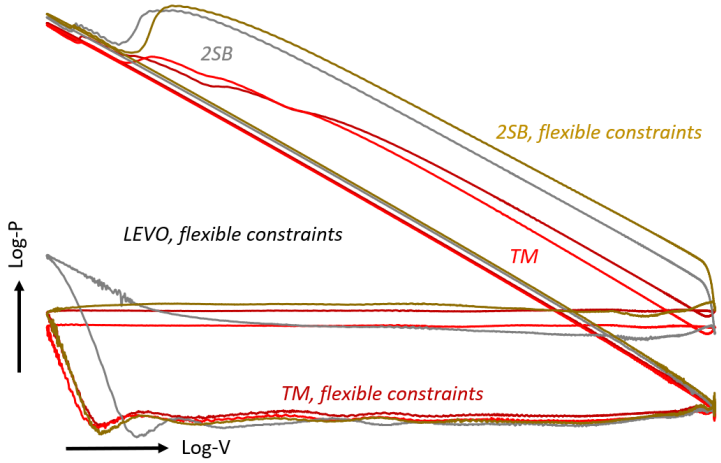

Figure 3.10. PV diagram for firing cylinders in flexible-constraint 2SB and flexible-constraint TM, compared to stock TM calibration.

Figure 3.11 likewise shows the PV traces for the non-firing cylinders in both 2SB cases. Again, the key differentiator is the higher exhaust pressure in the flexible-constraint case, stemming from a more-closed VGT.

3.5 Results and Discussion

At all four of these strategies (emissions-constrained and flexible-constraint variants of both 2SB and TM) were implemented on the VVA engine at 800 RPM, 1.3 bar BMEP. After allowing parameters to reach steady-state, a 30 second, 100 hz log was captured. The data reported here represents the average values of parameters over that 30 second window.

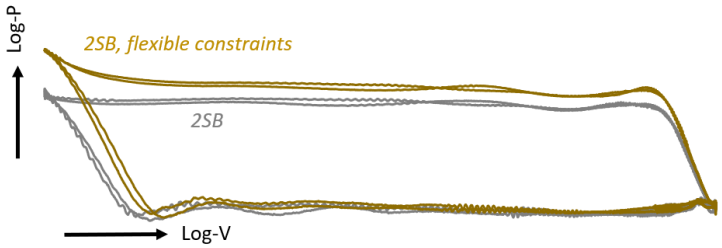

Figure 3.11. PV diagram for non-firing cylinders in flexible-constraint 2SB compared to emissions-constrained 2SB.

Also included are results from work done by Joshi [34] using LEVO. These results provide an interesting point of comparison, as while they have the same objective (faster warm up of the SCR) and employ the same technology (diesel engine VVA), they use a completely different approach. While 2SB focuses on increasing the mass flow rate of exhaust, LEVO focuses on increasing the temperature of exhaust while not significantly affecting the mass flow rate. While LEVO is not directly part of this work, the data is shown to provide contrast with a competitive technology. Two points are included; one emission-constrained (labeled "LEVO") and the other with flexible constraints (labeled "LEVO, flexible constraints").

Figure 3.12 provides results for the two most important parameters, exhaust mass flow rate (normalized to that of TM) and turbine-outlet temperature (TOT). 2SB, when given flexible constraints, is able to reach temperatures matching those of TM at a significant (75%) mass flow rate advantage. When meeting emissions constraints, 2SB sees a marginal mass flow rate drop, as well as a significant temperature penalty. As points of comparison, flexible-constraint TM achieves marginal TOT and exhaust flow rate benefits thanks a more-closed EGR, a more-closed VGT, and adjustments to the fuel injection strategy, while LEVO provides a meaningful temperature benefit and near-nominal exhaust flow when emission constrained but a significant temperature benefit when given flexible constraints.

This demonstrates clearly the differences in application between 2SB and LEVO as VVA strategies thermal management: LEVO can provide temperature benefit with little influence on exhaust flow and 2SB can provide increased mass flow benefit but not increased temperature.

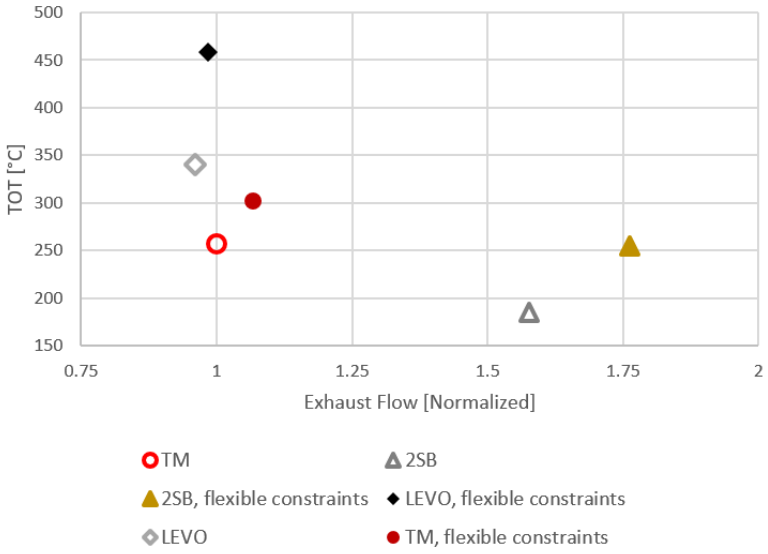

Figure 3.12. Turbine-out temperature vs exhaust mass flow rate for 2SB, TM, and LEVO at 800 RPM, 1.3 bar BMEP.

Figure 3.13 shows normalized steady-state engine-out emissions for all six thermal management strategies vs their normalized respective steady-state fuel consumptions, a particularly critical plot given that not all strategies meet the same constraints. 2SB and LEVO (the emissions-constrained cases) have NOx and PM flow rates below the bounds of the TM case. The flexible-constraint cases vary in the degree to which they exceed the TM constraints. Flexible-constraint 2SB produces the most NOx, followed by flexible-constraint TM, while flexible-constraint LEVO actually has in-bounds NOx. That said, LEVO produces the most PM of the flexible-constraint strategies, followed by 2SB and then TM.

It is also notable that all strategies pay a meaningful fuel consumption penalty. This is somewhat thermodynamically inherent; under most circumstances, creating

higher rates of heat transfer going to the exhaust will require extra fuel to be burned. This is demonstrated here, as additional temperature or mass flow (higher exhaust heat power) roughly correlates with fuel consumption. The degree of added fuel consumption will need to be balanced with the need for faster warm up, but given that these strategies will be employed for relatively short amounts of time (just enough to get the SCR hot), an decrease in warm up time may be worth the cost in fuel.

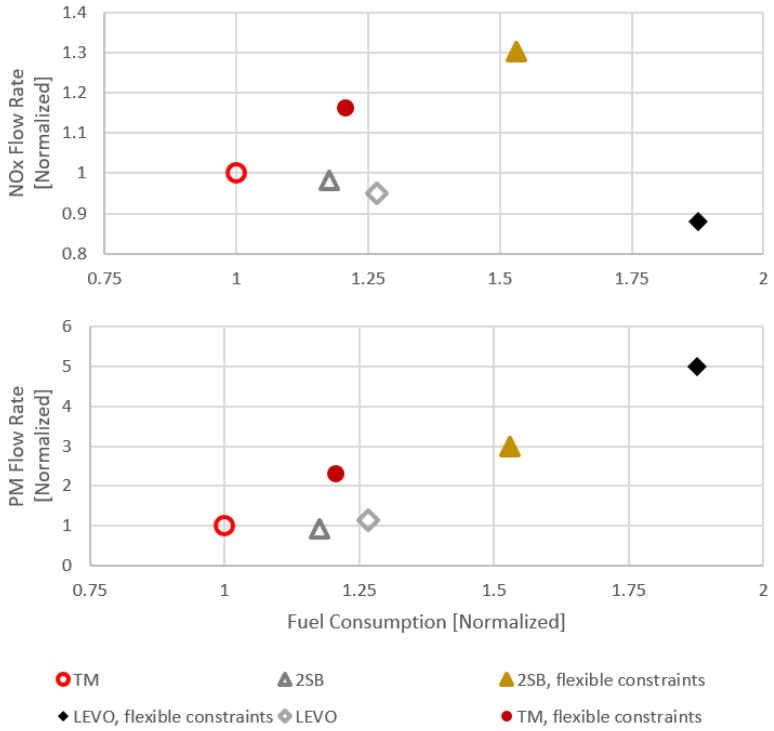

Figure 3.13. Engine-out NOx and PM emissions for 2SB, TM, and LEVO at 800 RPM, 1.3 bar BMEP.

Figure 3.14 presents a variety of additional data for the cases of interest, including intake manifold pressure (IMP), turbocharger shaft speed, and fresh air flow rate. Note that the fresh air flow rate increases more than the 1.5x that one would expect when doubling the number of strokes in half of the cylinders; rather, it is around 1.6x and 1.8x for emissions-constrained and flexible-constraint 2SB, respectively. It is hypothesized that this is due to the additional mass flow increasing the turbocharger

speed, and therefore the boost pressure, apparent in their respective plots. While LEVO also experiences higher IMP than TM, it does not see an increase in mass flow rate. This is probably due to differences in EGR fraction; very likely, less EGR is circulated in the 2SB cases than in the LEVO cases. However, this was never confirmed, as the split exhaust manifold presents challenges for the determination of EGR fraction with a heterogeneous cylinder strategy such as 2SB.

While mass flow rate and temperature are valuable metrics for evaluating thermal management performance of various strategies, it can be challenging to directly compare two different strategies where both mass flow and temperature are significantly different. For example, it is straightforward to predict that LEVO will heat the SCR faster than TM (as it has the same mass flow rate but a higher temperature), but more challenging to make such a determination between LEVO and 2SB.

Ding [40] proposed a simplified equation that models the relationship between steady-state TOT, steady-state exhaust flow rate, and heat transfer to the SCR catalyst:

$$\dot{q} \approx \dot{m}_{exhaust}^{\frac{4}{5}} C_p (TOT - T_{catalyst}) \tag{3.1}$$

where $\dot{q}$ is the rate of heat transfer from the exhaust gas to the SCR catalyst, $\dot{m}_{exhaust}$ is the steady-state exhaust mass flow rate, C_p is the heat capacity of the exhaust, TOT is the steady-state turbine-outlet temperature, and $T_{catalyst}$ is the lumped mass temperature of the SCR catalyst bed. While this is an approximation that makes a significant number of simplifications, it provides a framework to make comparisons between a wider variety of thermal management strategies, including the impact of instantaneous catalyst temperature.

Figure 3.15 shows the results of this model for heat transfer rate being applied to the cases of interest here, demonstrating the effectiveness of each at heating the SCR catalyst as a function of catalyst temperature. The higher the exhaust flow rate, the higher the slope of the line; the higher the TOT, the higher the y-axis offset. The point where each line crosses 0 on the y-axis denotes the equilibrium point, where

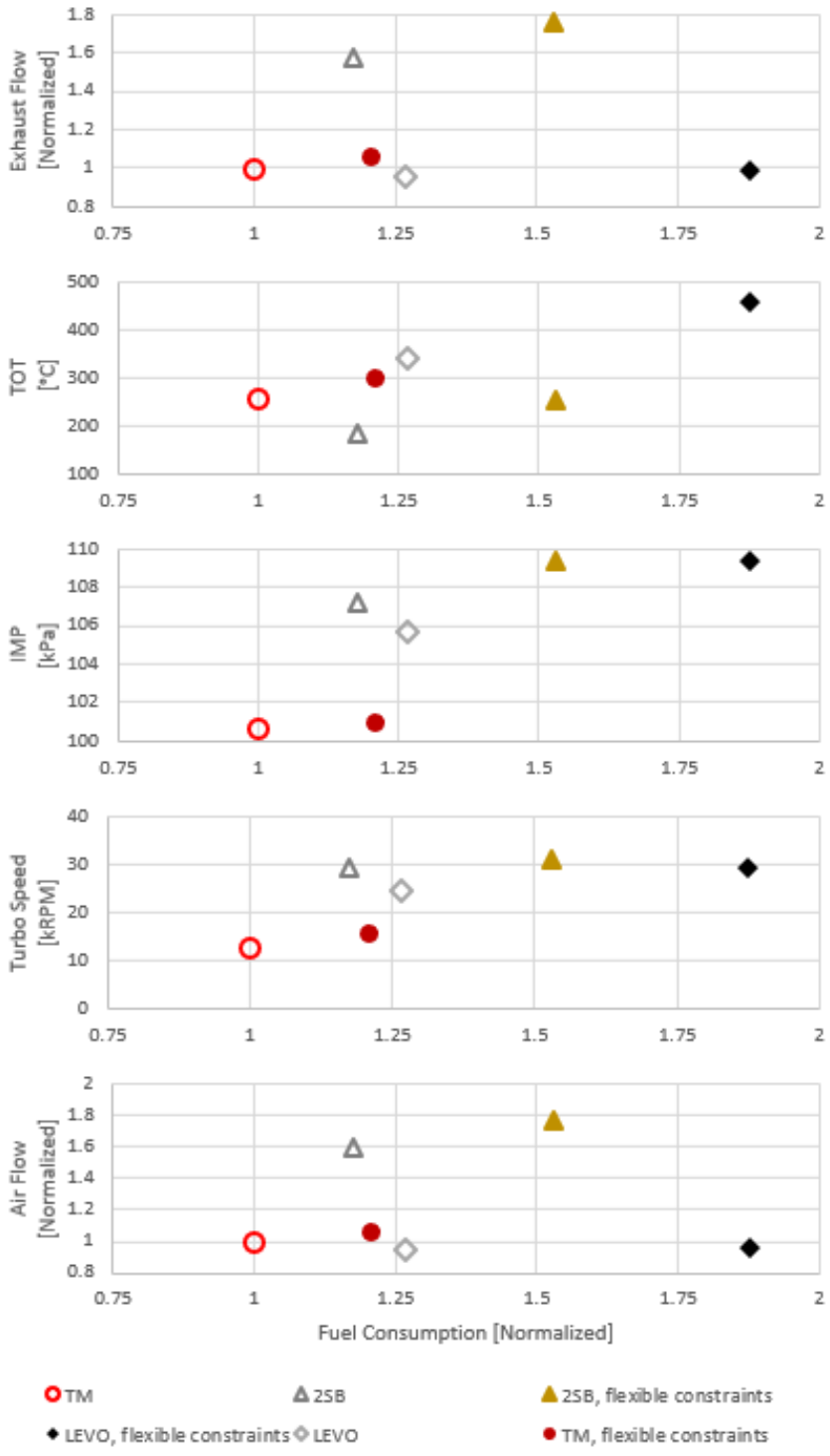

Figure 3.14. Experimental results for 2SB, TM, and LEVO at 800 RPM, 1.3 bar BMEP.

the exhaust and catalyst are at the same temperature. To the left of that point, the exhaust is heating the catalyst; to the right, the exhaust is cooling the catalyst. Obviously, the objective is to maximize the heat transfer rate from the exhaust gas to the catalyst over the 0-250°C range, as more heat transfer will heat the SCR up faster.

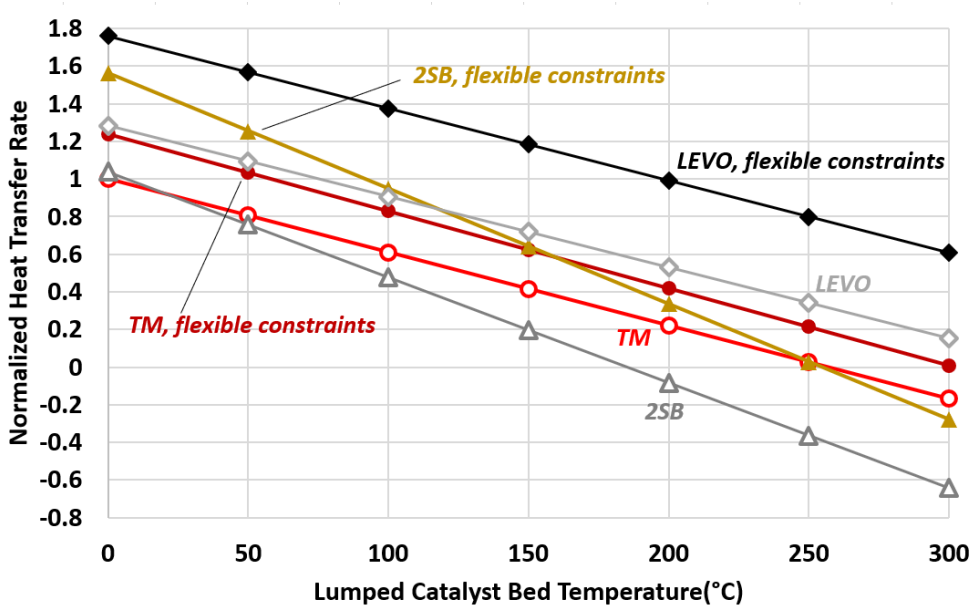

Figure 3.15. Approximate heat transfer rate from exhaust gas to catalyst bed, as a function of catalyst temperature.

While emission-constrained 2SB's performance with this model does not hold up to that of TM, flexible-constraint 2SB actually outperforms TM all the way up to 250°C, and outperforms flexible-constraint TM and emissions-constrained LEVO up until catalyst temperatures of 150°C and 120°C, respectively. Flexible-constraint LEVO, however, has the highest heat transfer rate across the whole board of SCR catalyst temperatures.

3.6 Summary

In order to decrease the time required after a cold start before SCR light-off (and thereby decrease cumulative tailpipe NOx), 2-stroke breathing (2SB) was presented, a diesel engine aftertreatment thermal management strategy that involves only injecting fuel and firing in three cylinders and breathing twice as fast as normal in the non-firing cylinders with 2-stroke valve profiles. While 2SB simulations predicted the resulting increase in exhaust flow rate could have thermal management benefits compared to a conventional thermal management strategy, experimental results show that when constraining emissions to those of the conventional strategy, the cold gas from the non-firing cylinders diluted the temperature of the exhaust flow significantly, enough that the modeled heat transfer rate to the catalyst predicted no advantage for 2SB relative to a conventional strategy.

However, when allowed to operate with increased engine-out NOx and PM flow rates, 2SB was shown to be able to match the engine-out temperature of the conventional strategy while maintaining a high mass flow rate, giving it a significant advantage in potential heat transfer to the SCR catalyst. A flexible-constraint version of the conventional strategy was created to demonstrate the SCR warm-up potential of the stock engine actuators; even compared to this strategy; flexible-constraint 2SB shows promise for high heat transfer to the SCR for catalyst temperatures below 150°C.

2SB was not able to match the warm-up potential of flexible-constraint LEVO, an alternative VVA strategy for faster SCR warm up. Still, it provides another tool in the toolbox for engine designers, should externalities make it favorable for reasons not considered here.

4. EXPERIMENTAL CHARACTERIZATION OF CLASS 8 TRUCK PLATOON DRAG COEFFICIENTS

4.1 Motivation

A key step in the development and introduction to market of platooning technology is gaining a further understanding of the aerodynamic effects of vehicles in a platoon on each other. To this end, a number of teams have performed experimental testing to determine the effects of platooning on the fuel economy of the lead and follow vehicle [23, 24, 41].

However, fuel economy results don't tell the entire story; characterization of aerodynamic drag coefficients is also essential, as drag coefficients are required for creating high-fidelity platooning simulations. Accurate simulations are crucial for the development of platooning controllers and algorithms, as simulations can be used to replace experiments for initial testing and calibration, leading to significant cost savings and much faster iteration. The more accurate the model, the less time will have to be spent doing experimental calibration.

A number of works in literature aim to provide characterizations of aerodynamic drag coefficients. These include both detailed computational fluid dynamics simulations [42, 43] and wind tunnel testing of scale models [44]. However, few studies employ modern tractor aerodynamic devices (such as those employed during experiments detailed in this dissertation) and, additionally, none of them provide full-scale experimental verification for their results. While these models are valuable, full-scale experimental results provide additional confidence, getting results closer to reality.

The chief challenge for full-scale aerodynamic testing is that the normal methodologies for conducting such tests on an individual truck cannot be easily applied to

platooning trucks. There are two ways this testing is normally conducted for a single truck: wind tunnel testing and coastdown testing.

Full-scale wind tunnel testing of platooning trucks is difficult because of the space required. Assuming experiments were to be performed on two sleeper cabs with 53' trailers (the typical case analyzed in fuel economy testing), testing even at just a 50' gap would require a test section around 200' long. If there is a wind tunnel in operation that can accommodate this size, it would have to be among the largest in the world.

Coastdown testing presents its own set of issues. The SAE J2263 coastdown testing procedure requires that the engine be disengaged from the transmission and that the brakes are not used. However, without the engine or brakes there is no method to control the gap between the trucks. As the rear truck experiences less aerodynamic drag, it would maintain speed longer than the front truck, and the two would collide. Mechanical coupling between the two trucks could be used to control the gap during the coastdown, but then this mechanical interaction between the two trucks would need to be measured and accounted for in the calculations.

The following presents an alternative, more practical framework for experimentally determining the drag coefficients of class 8 trucks in a two-truck platoon, and implements that process for MY2019 Peterbilt 579's in a platoon

4.2 Method for Calculating Platoon Drag Coefficients

This methodology is built around a energy balance for a vehicle traveling from a hypothetical point 1 to point 2:

$$\Delta KE_{12} + \Delta PE_{12} + W_{12} = 0 \tag{4.1}$$

If the vehicle travels in a closed-loop, such that points 1 and 2 are the same location (for example, the start/finish line on an oval track), there is no net change

in elevation, so the change in potential energy is zero. Likewise, if the vehicle speed is the same at point 1 as it is a point 2, the change in kinetic energy is zero.

$$\cancel{\Delta KE_{12}} + \cancel{\Delta PE_{12}} + W_{12} = 0 \tag{4.2}$$

Thus, the only remaining term is the net work acting on the vehicle from point 1 to point 2, which (neglecting driveline friction and other small forces) can be broken down into brake engine work, aerodynamic work, and rolling resistance work:

$$W_{12} = 0 = W_{engine} - W_{aerodynamic} - W_{rolling} \tag{4.3}$$

which can the be broken down further:

$$W_{12} = 0 = \int_1^2 \tau_{engine}\dot{\phi}_{engine}dt - \int_c F_{aerodynamic}ds - \int_c F_{rolling}ds \tag{4.4}$$

where τ_{engine} is brake engine torque, $\dot{\phi}_{engine}$ is engine angular velocity, $F_{aerodynamic}$ is the aerodynamic force, $F_{rolling}$ is rolling resistance force, and s is the distance traveled.

As long as the platooning strategy being analyzed has a constant gap between the trucks and the change in vehicle speeds are small, aerodynamic drag force is assumed to be constant. If the rolling resistance force is also approximated as constant, the integrals can be simplified:

$$W_{12} = 0 = \int_1^2 \tau_{engine}\dot{\phi}_{engine}dt - F_{aerodynamic}s - F_{rolling}s \tag{4.5}$$

and aerodynamic drag and rolling resistance can be broken down using their defining equations:

$$W_{12} = 0 = \int_1^2 \tau_{engine}\dot{\phi}_{engine}dt - \frac{C_d A \rho_{air} V^2}{2}s - (C_{rr} m_{vehicle} g)s \tag{4.6}$$

further rearranging to solve for C_d:

$$C_d = \frac{2}{A\rho_{air}V^2 s}\left(\int_1^2 \tau_{engine}\dot{\phi}_{engine}dt - (C_{rr} m_{vehicle} g)s\right) \tag{4.7}$$

where C_d is the vehicle coefficient of drag, A is the vehicle frontal surface area, ρ_{air} is the density of air, V is the average velocity of the vehicle, C_{rr} is the coefficient of rolling resistance, $m_{vehicle}$ is the vehicle mass, and g is acceleration due to gravity.

What makes this equation particularly compelling is the availability of all the required data. Engine speed, engine torque, velocity, and distance are commonly logged in any type of vehicle testing, area and mass are typically known vehicle parameters, and air density can be determined as a function of ambient temperature. The only challenging parameter is the coefficient of rolling resistance, which can be determined through a single truck coastdown test or potentially provided by tire manufacturers, as it will be the same for a platoon as it is for a single truck.

The test procedure is also relatively simple: laps just need to be run around an oval track at a constant speed, both with a single truck and with a fixed-gap platoon. The recorded engine speed and torque data can then be used with Equation 4.7 to calculated the drag coefficient for each case.

Note that Equation 4.7 only considers static rolling resistance (dynamic rolling resistance is not included) and does not account for variations in the aerodynamic yaw angle. These simplifications (and the others described above) are meant to enhance ease of use; however, with some modifications to the derivation, it is possible some of these simplifying assumptions could be removed to add additional detail.

4.3 Platoon Drag Coefficients

The experimental data used for the analysis here was actually taken from a dataset collected during SAE J1321 Type II fuel economy tests. Two independent tests were conducted in August and December of 2019 at the Continental Proving Grounds in Uvalde, TX, using the trucks and instrumentation described in Chapter 2. Figure 4.1 shows a satellite image of the Uvalde track.

The larger, outer oval was used for testing and is approximately 13670m long (8.5mi). The start/stop location is marked on the figure; only “hot laps” were used

Figure 4.1. Satellite image of the Continental Proving Grounds in Uvalde, TX, with start/finish location marked on the outer oval.

for calculations, excluding the first and last lap of each set to ensure constant vehicle velocity for the duration. The trucks were operated with the OEM cruise controller set to 65 mph and the platoon gap controller set to 55 ft. As the data was collected as part of a fuel economy test, tire pressures were frequently calibrated and other vehicle parameters pertinent to J1321 were closely monitored.

The August test data includes 7 laps worth of single truck testing for each truck (14 laps total) and 22 laps for the platoon. The December data includes 22 laps of single truck testing for each truck (44 laps total) and 15 laps for the platoon. All vehicle parameters used in these calculations were measured, excluding the coefficient of rolling resistance, which was estimated based on typical rolling resistance values for class 8 trucks, and air density, which was determined as a function of measured ambient temperature.

An example single-truck lap is shown in Figure 4.2. Note that velocity and elevation have the same value at the end as they do at the beginning, since the start and

the finish are at the same point on the oval. This is essential in order to apply the assumption that change in kinetic and potential energy from start to finish is zero. Further note that the variation in velocity is small, ±1 m/s. With smaller variations in velocity, less fidelity will be lost when modeling drag force as constant.

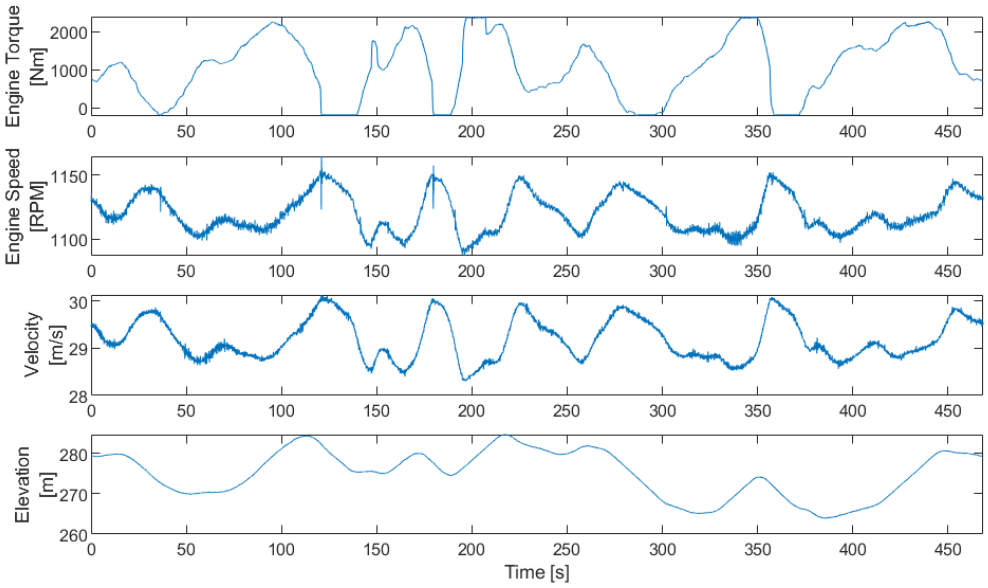

Figure 4.2. Engine torque, engine speed, vehicle velocity, and elevation for a single lap of the Uvalde track.

To check data repeatability, aerodynamic work for each lap was calculated by rearranging Equation 4.7:

$$W_{aerodynamic} = \int_1^2 \tau_{engine}\dot{\phi}_{engine}dt - (C_{rr}m_{vehicle}g)s \tag{4.8}$$

and is plotted in Figure 4.3, demonstrating the variation in aerodynamic work both from lap to lap and between the two different test sessions. While the trends are similar from August to December, there was a significant change in the actual value of the aerodynamic work. Averaged between the three test cases, there was an 8.1% increase in aerodynamic work from August to December. While the trucks

were not modified in any way between the two tests, there was a large difference in ambient temperature between the tests: the daily average was roughly 100°F in August compared to 60°F in December, meaning there was a 7.8% increase in air density from August to December. The denser the air, the harder the vehicles have to work to move through the air, increasing the aerodynamic work required for one lap. However, air density is accounted for in Equation 4.7, so the change in density should not affect the calculation of drag coefficients.

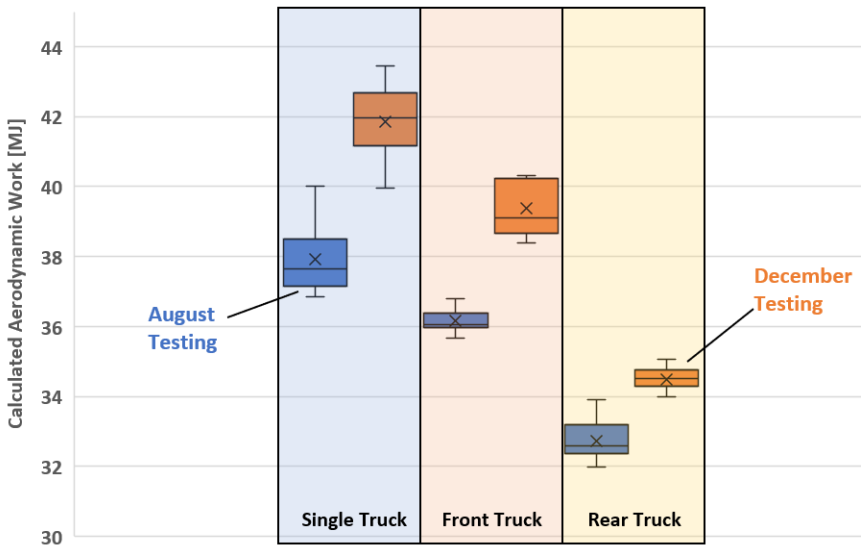

Figure 4.3. Variation of aerodynamic work per lap, using an estimated coefficient of rolling resistance.

Figure 4.4 shows the drag coefficients, calculated using Equation 4.7. The variation from August to December is very small (1.8% on average), indicating good repeatability. The average of the two data sets is also shown; these are the final values selected for use in simulations going forward. The front truck drag coefficient represents a 5.1% reduction vs a single truck, and the rear truck drag coefficient represents a 15.5% reduction vs a single truck.

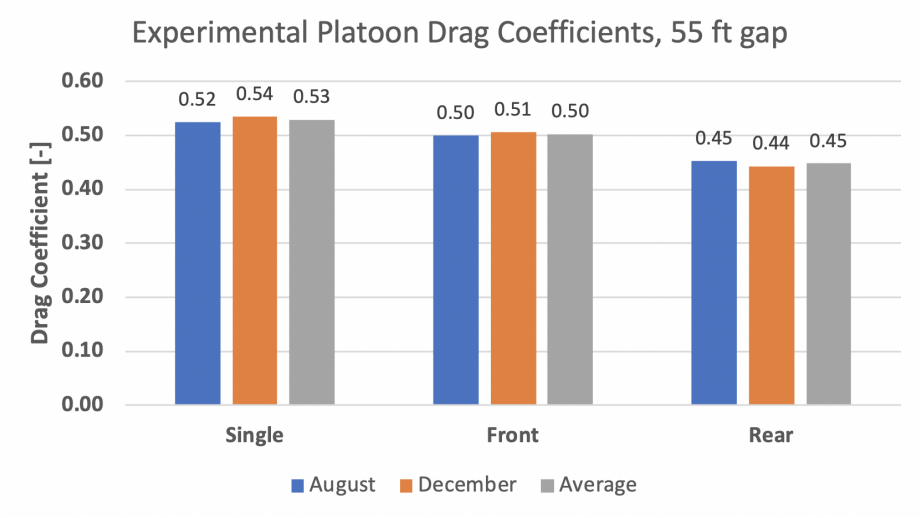

Figure 4.4. Experimentally determined drag coefficients for platooning trucks with a 55 ft gap, using an estimated coefficient of rolling resistance.

4.4 Summary

In order to improve the accuracy of platooning vehicle simulations, an experimental methodology was presented for determining platoon drag coefficients. This method is designed to be implemented with platoon test data recorded on an oval track, with the trucks at a constant speed and a constant platooning gap.

Analysis was conducted of experimental data of MY2019 Peterbilt 579's in a platoon with a 55 ft gap. The single truck (no platoon) drag coefficient was determined to be 0.58, while the drag coefficient of the front truck was determined to be 0.55 (5.1% drag reduction) and the drag coefficient of the rear truck was determined to be 0.49 (15.5% drag reduction).

One potential advantage of this method is that it could easily be retroactively applied to existing data closed-track J1321 fuel economy testing. Experiments have been conducted by other researchers at a variety of speeds and platoon gaps; those data could be analyzed using this framework to back-calculate drag coefficients, mak-

ing a much more complete picture than the single speed/gap combination studied here.

5. IMPLEMENTATION OF A VARIABLE GAP PLATOON CONTROLLER ON A CLASS 8 TRUCK

5.1 Motivation

As discussed in section 1.2.2, there are several challenges to overcome when platooning on hilly terrain with steep road grades. One is controlling gap during transitions into steeper uphill grades; with conventional platoon controllers, the gap between the trucks can grow, encouraging other vehicles to cut-in and disrupt the platoon. Another is controlling gap on long downhill grades; since the rear truck experiences less aerodynamic drag, the vehicle engine brake use is commonly used to maintain the minimum safe spacing, which converts vehicle energy to heat, increasing overall route fuel consumption.

As discussed in section 1.3.2, Ibitayo [36] proposed a variable gap two-truck platoon controller to address both these issues. Rather than working to maintain a constant spacing between the trucks, this controller allows the vehicle gap to grow or shrink within defined limits, using an MPC optimizer to determine the most fuel-efficient spacing for the trucks at each point on a route based on grade and speed limit information. Figure 5.1 shows three such gap profiles, generated between a lower limit of 16.7m and upper limits of 25, 30, and 40m, for a 52 km section of I-69 in southern Indiana with a 65mph speed limit.

Ibitayo implemented these profiles in simulation using a MPC gap controller, which uses a vehicle model and look-ahead route data to predict the engine torque required from the rear truck to track the desired gap profile. This framework is shown in Figure 5.2. Simulations predicted somewhat of a tradeoff between fuel efficiency and minimizing gap to prevent cut-in's; 30m and 40m had 7% rear truck fuel savings, but obviously require allowing more truck spacing growth. The 25m profile still saw

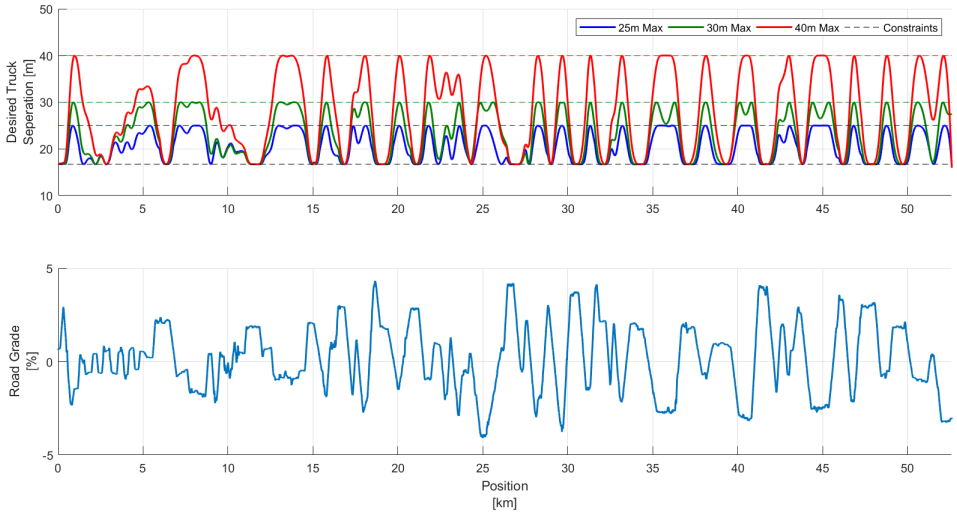

Figure 5.1. Variable platoon gap profiles proposed in [36] for reducing fuel consumption and controlling gap growth on a heavily-graded section of I-69.

6% rear truck fuel savings, but actually reduced the maximum gap throughout the route by 9m compared to the production-intent controller, meaning it is effective as both a fuel-saving strategy and a gap-control strategy.

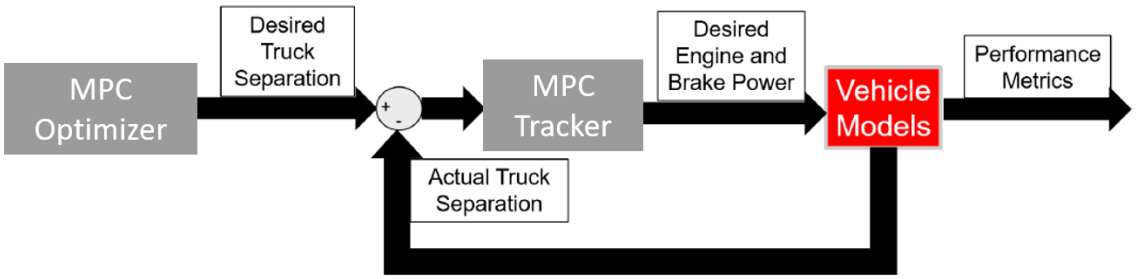

Figure 5.2. Diagram of Ibitayo's variable gap controller framework. The gap profile is pre-generated by the MPC Optimizer and that profile is tracked using the MPC Tracker.

Figure 5.3 demonstrates how a variable gap platoon controller can help save fuel compared to a conventional platoon controller. This section of route includes an uphill grade from 0.2 km to 0.6 km followed by a downhill grade from 0.6 km to 1.2 km. During the transition from uphill to downhill, the front truck pulls away from the rear truck in both cases. The production-intent controller keeps the rear truck torque high to catch back up (until 0.8 km), but then needs to use the retarder (negative engine torque) on the downhill section in order to maintain a safe minimum gap. On the other hand, the variable gap optimizer knows that a downhill section is coming up, and created a gap profile for the MPC tracker to follow that uses the downhill grade to help the rear truck catch up instead of extra engine torque, eliminating the need for retarder use.

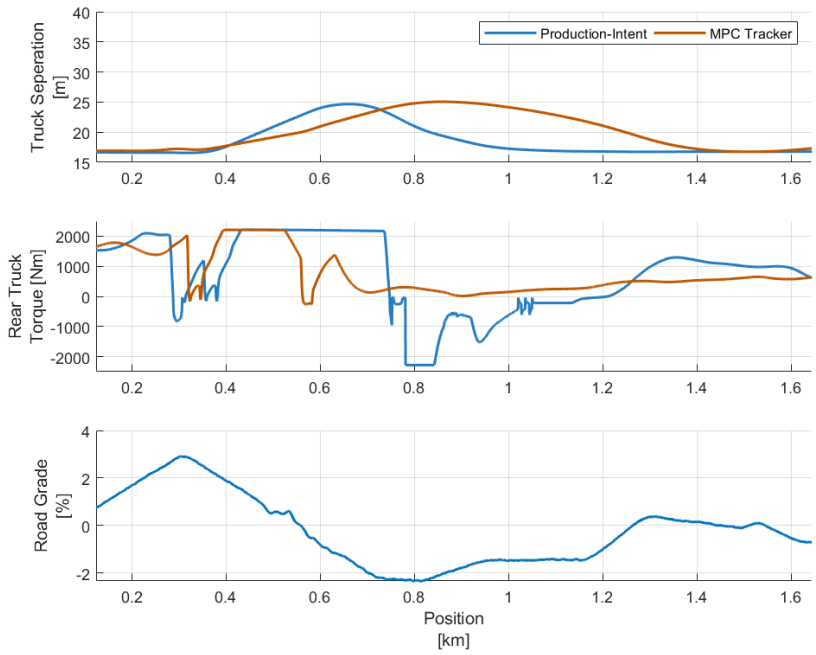

Figure 5.3. Example showing variable gap platooning's ability to reduce retarder use by leveraging look-ahead grade data.

Figure 5.4 demonstrates how a variable gap controller can also help limit gap growth. This section includes a transition from a mild uphill grade (16 km to 16.5

km) into a steep uphill grade (16.5 km to 17km). When the front truck enters the steeper grade and slows down slightly, the production-intent controller uses some retarder to slow the rear truck to keep the gap constant. This means that it has less momentum when it enters the steeper grade, causing it to slow down to a lower speed than the front truck did. Since torque is saturated, the gap grows until rear truck crests the hill. The variable gap optimizer knows that a steep uphill section is coming, so it created a gap profile for the MPC tracker to follow that includes a slight dip right at 16.5 km so that the rear truck doesn't need to hit the brakes to slow itself down before being slowed down by the hill, allowing it to maintain the same momentum as the front truck and keep the gap small.

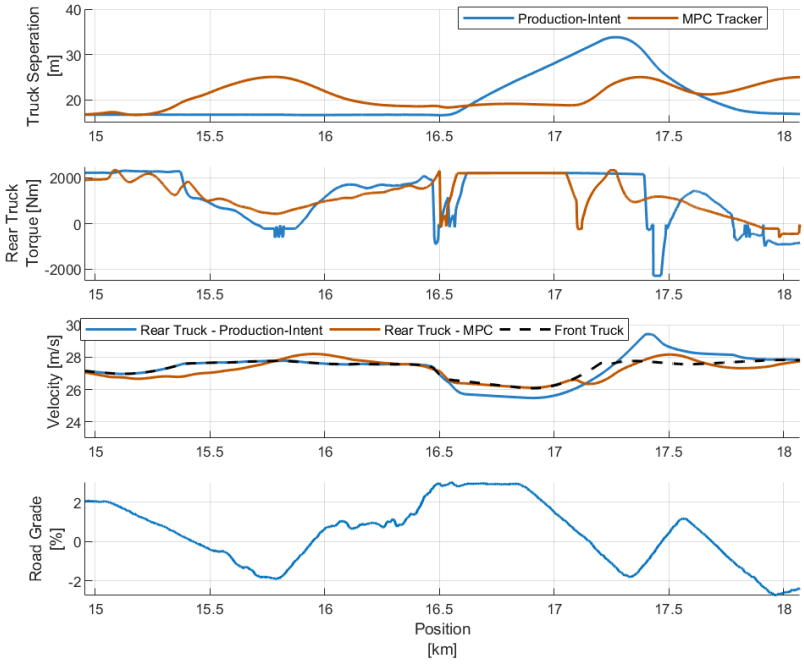

Figure 5.4. Example showing variable gap platooning's ability to control gap growth.

In both these regards (gap control and fuel efficiency), the MPC tracker does very well; use of look-ahead data helps it track the gap profiles very accurately. However if a variable gap controller is to be implemented on real trucks, processing power

requirements also need to be considered. Figure 5.5 shows the computation times of the MPC tracker on a desktop machine with performance specifications that meet or exceed those of the intended prototype computer. For real-world implementation, computation needs to happen faster than real-time, i.e., the total computation time divided by the length of route computed should be less than 1. The MPC tracker, as implemented in simulation, runs significantly slower than real-time.

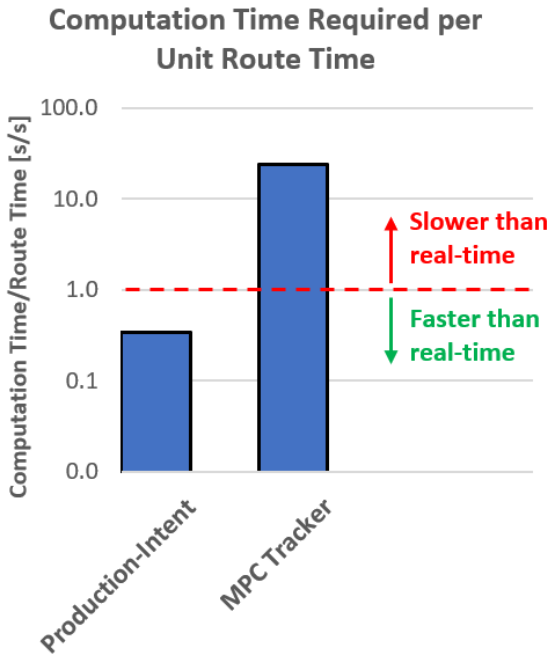

Figure 5.5. Amount of time required for computation of each second of the route on example hardware. Production-intent included for comparison.

In order to speed up computation and to meet a tight schedule, an alternative, simplified controller was developed, designed for computational efficiency as well as ease of implementation and calibration. The following describes the development and testing of that controller, and provides a performance comparison to the MPC tracker and results of fuel economy simulations.

5.2 Controller Design and Simulation Testing

The first phase of development was testing in simulation. A high-fidelity blackbox vehicle model representative of the trucks to be tested was used, including transient and steady-state engine torque/fuel maps and a transmission/driveline model, as well as the effects of drag, rolling resistance, grade, and braking. A schematic of the simulation is shown in Figure 5.6.

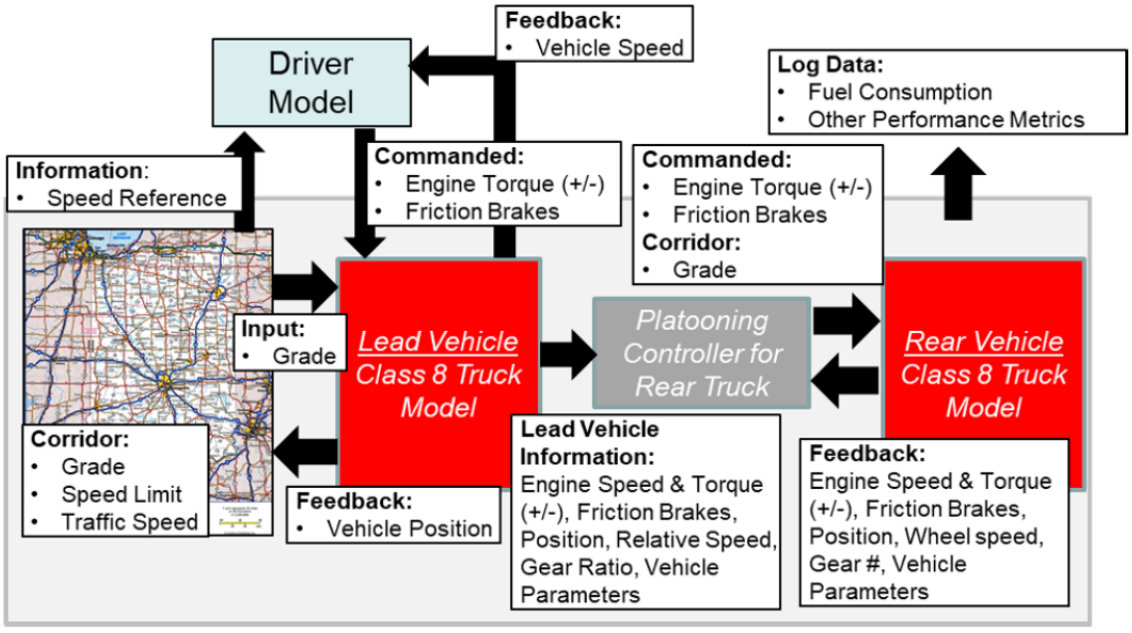

Figure 5.6. Schematic of the high-fidelity vehicle model used for testing.

The initial controller design was a simple PI compensator with the front truck torque as a feedforward, using the error between desired and measured gaps as an input and outputting a torque request. Gain calibration was initially performed on a flat route. First run of the controller was to be on a closed-course at the Continental Proving Grounds in Uvalde, TX, so grade data from the test track there was used for further simulation testing (more detail on the track is provided in chapter 4). The

MPC optimizer was used to generate gap profiles for the Uvalde track, and the new controller was used in simulation to track them.

Figure 5.7 shows the performance over several different controller configurations over the Uvalde route, including the original PI controller (labeled "PI"), a controller with an added derivative term (labeled "PID"), and a controller with both the derivative term and a proportional control on the relative velocity between the front and rear trucks (labeled "PID+"), all utilizing the front truck torque as a feedforward.

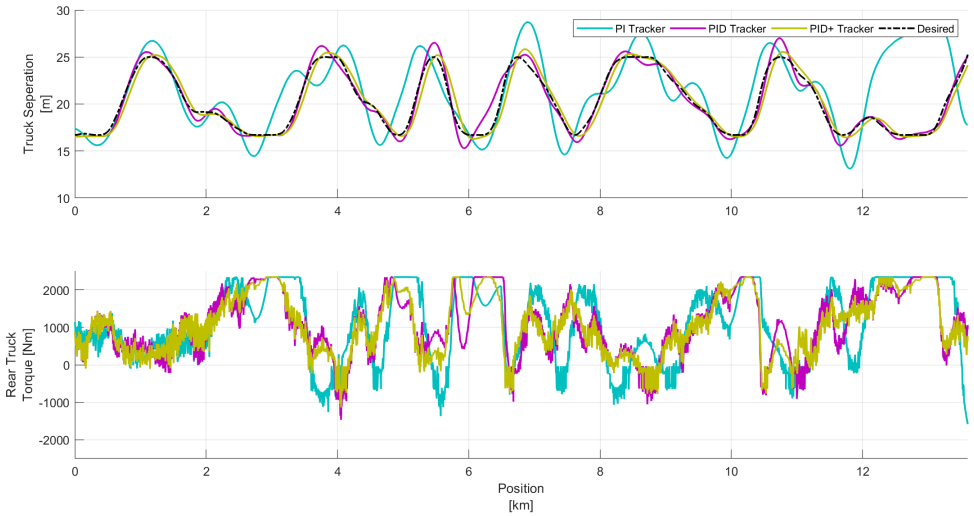

Figure 5.7. Simulated behavior on the Uvalde track for several different gap controller configurations.

Minimizing overshoot is critical to prevent the vehicle safety systems from activating the retarder when operating near the minimum gap and to prevent the gap from growing large enough to automatically dissolve the platoon when operating on a 40m profile. As it had the least amount of overshoot, the PID+ design was selected for functional testing in Uvalde.

Figure 5.8 shows the computation time required, comparing the MPC tracker to the PID+ controller. The PID+ is several orders of magnitude faster than the

MPC, making it faster than real-time and therefore a suitable candidate for vehicle integration.

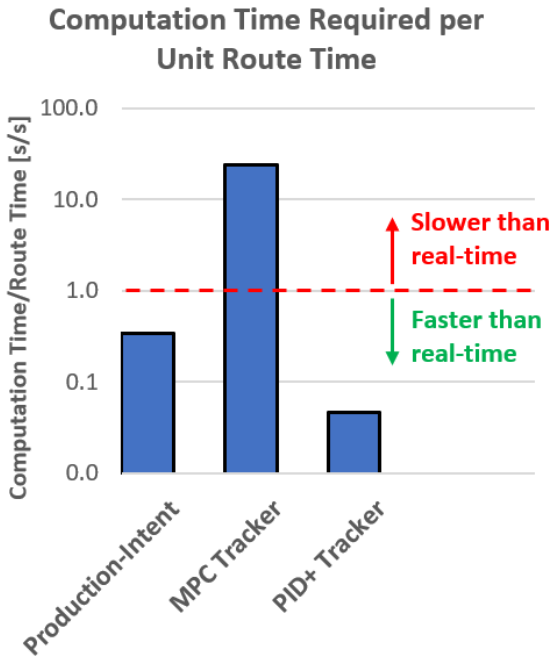

Figure 5.8. Amount of time required for computation of each second of the route on example hardware. Production-intent included for comparison.

5.3 Experimental Testing

After simulation testing, the PID+ controller was implemented on the truck for functionality testing in Uvalde. Tests consisted of getting both trucks up to speed, engaging the platoon, running a full lap with the production-intent controller, and then activating the variable gap PID+ controller tracking the profiles generated for Uvalde by the MPC optimizer. 25m, 30m, and 40m profiles were all vetted, with focus on the 25m and 40m profiles.

Over the course of the functionality testing, a significant amount of time was spent troubleshooting and correcting bugs in the code. Once everything was working correctly, controller gains were fine-tuned to improve qualitative tracking consistency.

Figure 5.9 shows an example test conducted with the 40m gap profile. Tracking was reasonably well maintained the entire time and consistent between the two laps. Note that the oscillations at the beginning of lap 1 were caused by an error with the code related to switching the tracker on and off (that has since been corrected) and lap 2 was cut slightly short. Neglecting those two incidents, the number of retarder-on events is reduced compared to the baseline controller, indicating potential for fuel savings. This route is not steep enough to evaluate gap control effects (production-intent controller already does not significantly deviate from the setpoint).

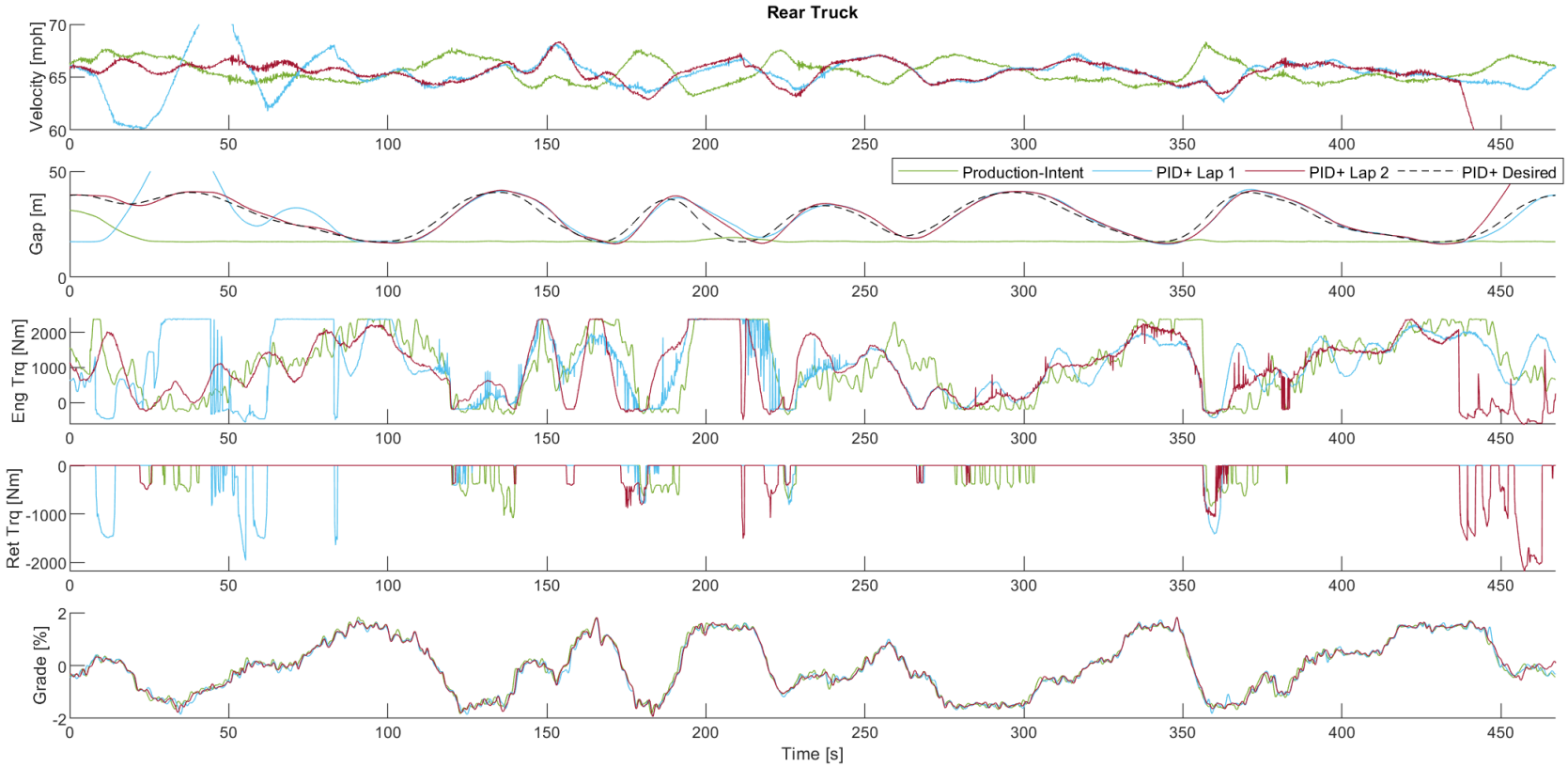

Figure 5.9. Experimental rear truck behavior on the Uvalde track for a 40m maximum gap.

In an attempt to further reduce retarder usage, a rule-based deadband was added to the controller, visualized in Figure 5.10. It was observed that in some cases, the retarder would activate even though the rear truck was only slighty closer to the front truck than desired. The objective was to create a deadband where the retarder would not activate if the error was less than a set amount, encouraging the truck to coast rather than using the retarder and potentially conserving some kinetic energy.

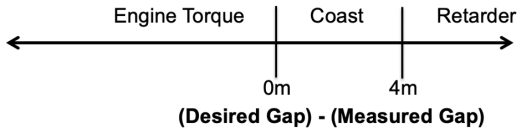

Figure 5.10. Deadband configuration, where the engine coasts (rather than using the retarder) if the gap error is less than 4m.

Figure 5.11 shows two laps of testing with a 4m deadband activated. While the deadband did help eliminate retarder use almost entirely on lap 2, on lap 1 it created a significant departure from the desired gap profile, leading to uncontrolled gap growth and a period of gap oscillation, behavior that was observed quite a few times. This effect would likely be even more pronounced on a steeper grade (like I-69), where a small change in momentum into a hill can make a large difference in gap management. While it may be a useful tool in some applications (especially if made smaller), it was not ultimately added to the final PID+ controller.

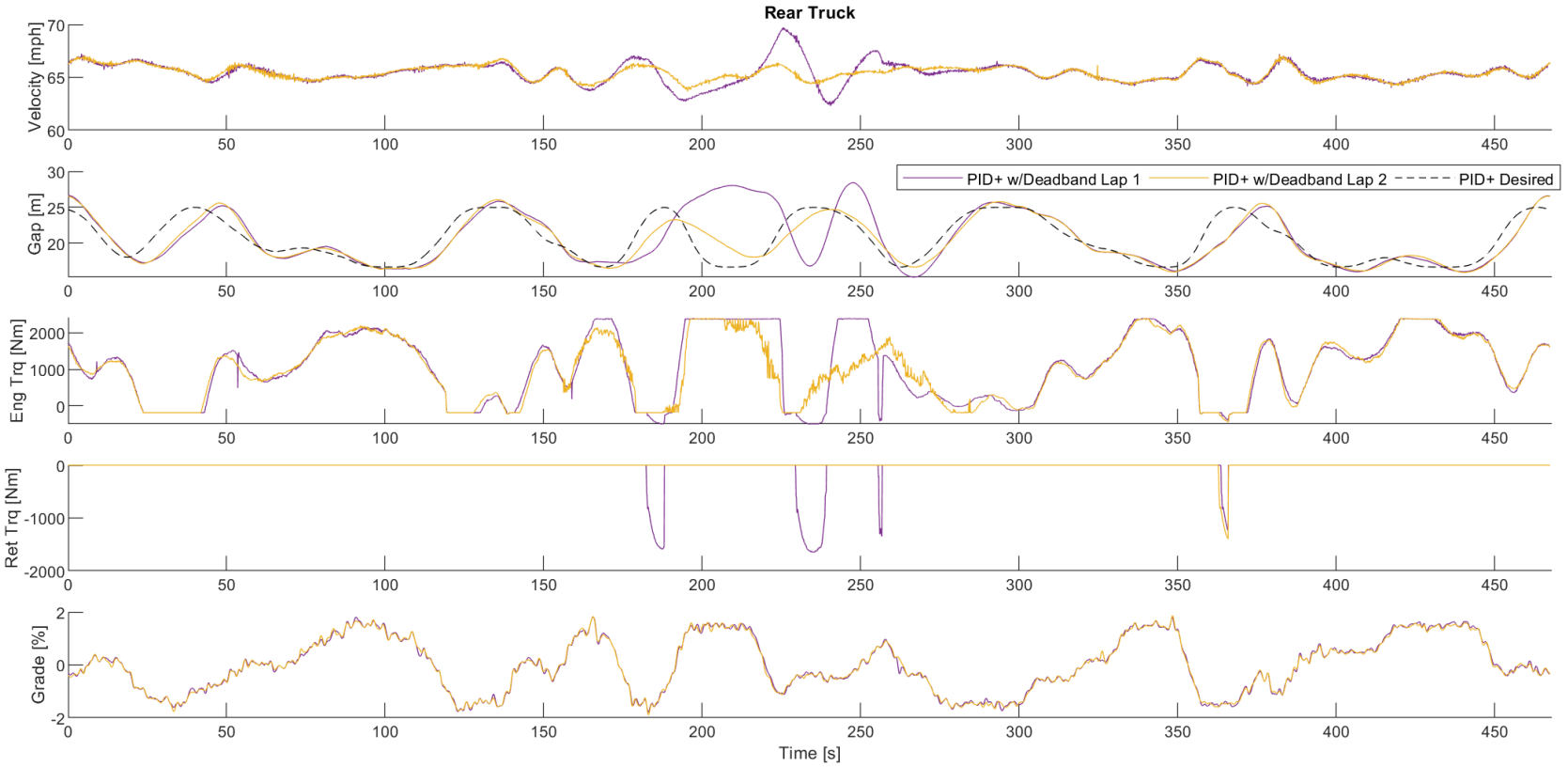

Figure 5.11. Experimental rear truck behavior on the Uvalde track for a 25m maximum gap with a 4m deadband.

5.4 Results and Discussion

After adding the adjustments made in Uvalde to the simulation model of the controller, simulations were ran over the I-69 grade for a more quantitative assessment of controller performance. Figure 5.12 shows gap and torque simulation results for all three profiles.

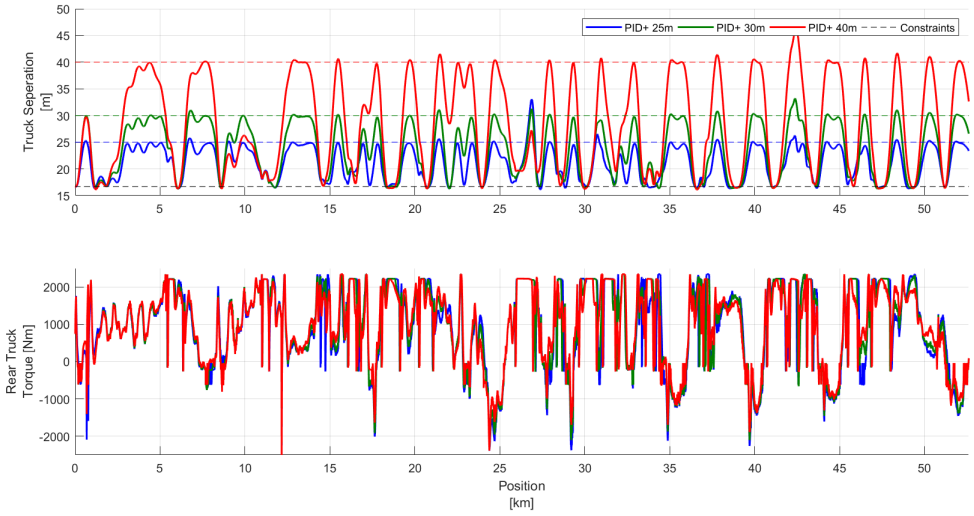

Figure 5.12. Updated simulation results for I-69 using the PID+ tracker with 25m, 30m, and 40m maximum gaps.

Figure 5.13 compares the finalized PID+ controller with a 25m profile to the production-intent controller. Note in particular that even though I-69 is a more steeply-graded route than the Uvalde track, tracking looks very consistent, with only one significant departure around 26 km.

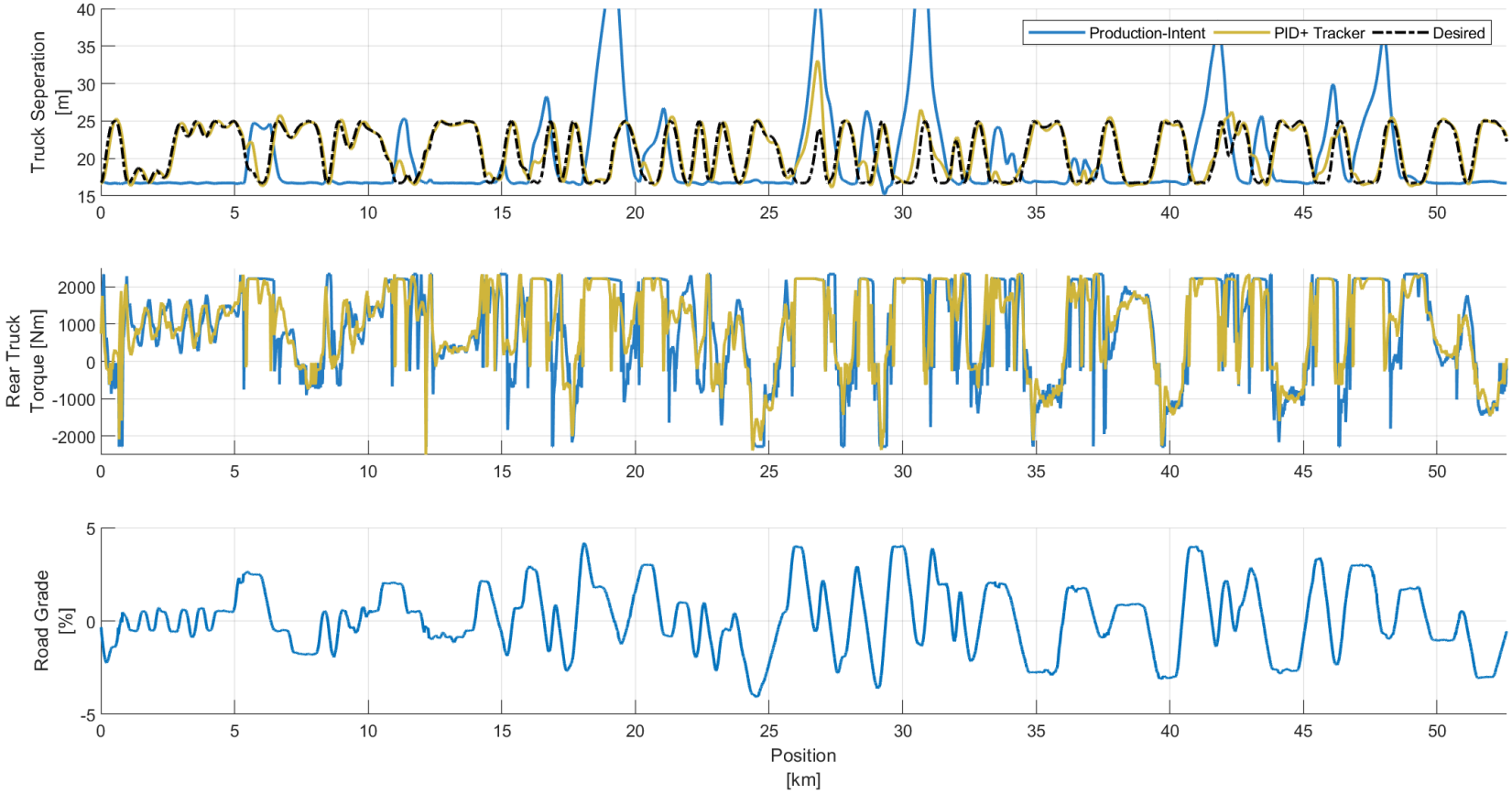

Figure 5.13. Updated simulation results for I-69, with the PID+ tracking a 25m maximum gap profile compared to a production-intent controller.

Table 5.1 shows results of the I-69 simulations compared to the production-intent controller. Use of the PID+ controller is projected to enable rear truck fuel savings of 6-9%, with reductions in maximum gap of up to 18m, marking improvements in both fuel consumption and gap control simultaneously. The fuel consumption of the front truck is consistent between cases (as the effects of this strategy on the front truck are minor), but the rear truck fuel consumption varies depending on the maximum allowed gap, with more gap variation achieving lower fuel consumption, at a trade-off with maximum gap.

Table 5.1. Simulation results for I-69 comparing PID+ to production-intent controller. Fuel consumptions normalized to the single truck case.

	Normalized Front Truck Fuel Consumption	**Normalized Rear Truck Fuel Consumption**	**Maximum Gap [m]**
Single Truck	1.00	-	-
Production-Intent	0.98	1.00	50.9
PID+, 25m	0.98	0.94	33.1
PID+, 30m	0.98	0.93	33.2
PID+, 40m	0.98	0.91	46.4

5.5 Summary

Previous work has shown that in a two-truck platoon, allowing the truck separation gap to vary can be advantageous from fuel economy and gap control perspectives. However, the significant processing power required for the existing MPC-based controller meant it would have been challenging to implement on a real truck.

An alternative, PID-based controller was proposed to track a pre-calculated desired gap profile. The controller was tested and calibrated in simulation, then imple-

mented on a truck, where functionality was experimentally demonstrated in closed-course testing.

Simulations show the PID controller is projected to have rear truck fuel savings of 6-9% compared to the production-intent controller on a heavily-graded real-world route (depending on the maximum gap allowed) and reduce maximum gap departure by up to 18m.

6. CONCLUSION

6.1 Summary

Commercial vehicles in the United States account for a significant fraction of greehouse gas emissions and NOx emissions. In the interest of reducing these emissions, this work presents a diesel engine VVA steady-state control strategy aimed at reducing tailpipe NOx emissions, a methodology for characterization the aerodynamic drag of platooning vehicles that can be used to create more accurate simulations and accelerate development of platoon controllers, and a platoon gap controller designed to reduce rear truck fuel consumption and increase control over the platoon gap.

The diesel engine strategy centers around using 2-stroke breathing to elevate exhaust mass flow rates, which can help heat up the SCR catalyst after a cold start so it can start converting NOx earlier. While emissions-constrained operation saw increases in mass flow rate negated by a corresponding drop in exhaust temperature, allowing the emissions constraints to "flex" allowed the strategy to operate at similar temperatures to the baseline but with exhaust flow rates 1.75x those of the baseline, which would increase heat transfer to the catalyst below catalyst temperatures of 250°C. This could help the catalyst heat up faster and potentially reduce tailpipe NOx, even with a slightly elevated NOx flow rate.

Platooning is a vehicle control strategy that has potential for enormous fuel savings if implemented in scale. In order to make fuel economy predictions and decrease development time for new platoon controllers, accurate platooning simulation models are an invaluable tool. These simulations can be made more accurate with aerodynamic drag coefficients derived from full-scale experimental testing. However, methods used for such characterizations on single trucks are challenging to adapt to platooning trucks. Therefore, a novel methodology for characterizing aerodynamic

drag for platooning trucks using on-road vehicle test data was developed. Drag coefficients for Peterbilt 579 tractors in a platoon were characterized at 65mph with a 55' gap, but this method could potentially allow others to backcalculate aerodynamic drag coefficients using existing data from J1321 platoon tests, enabling the construction of more accurate platoon simulations.

Previous work has shown that allowing the gap setpoint between the trucks to vary dynamically can help control gap and maximize fuel savings on hilly terrain, employing a MPC controller on the rear truck for tracking the desired gap profiles in simulation. However, this MPC controller provided challenges for implementation in a real truck. An alternative PID-based controller was developed, calibrated in simulation, and tested in a closed-course functionality test. This controller is predicted to achieve 6-9% rear truck fuel savings vs a production-intent controller on a heavily-graded I-69 route in southern Indiana, while reducing the maximum truck gap by as much as 18m. Reducing the maximum truck gap can help prevent other vehicles from cutting in between, which forces the platoon to dissolve.

6.2 Recommendations for Future Work

This work is not the end of the story for any of these ideas. The following recommends some suggested next steps for the projects involved.

Running the 2-stroke breathing VVA strategy at idle during a HD-FTP drive cycle will give a critical performance measure. This would demonstrate more concretely where 2SB could be employed with success and whether or not the added engine-out emissions are worthwhile from a tailpipe-NOx perspective. Additionally, it would be really interesting to try to get enough compression in the 2-stroke cylinders to burn a small bit of fuel; not to produce power, but to create a little additional temperature. Potentially, one could do almost a full compression stroke, inject and burn a small amount of fuel, then have a short exhaust profile just before or after TDC, followed by the intake stroke.

For further experimental drag coefficient characterization of platooning vehicles, it would be useful to run more tests like the ones described here but at a variety of gap distances. This could even be done with data from past J1321 oval track tests, if said data were made available. Additionally, this methodology could be validated by running a J2263 coastdown test.

Unlike the MPC tracking controller, the PID+ controller does not use any look-ahead data, and could be improved potentially by including proportional gains on the error between the grade coming up in some distance and the current rear truck grade or on the error between the front truck velocity coming up in some set distance and the current rear truck velocity. While this may be challenging to calibrate (as both the gains and the look-ahead distance need to be considered), it would be relatively simple to implement in simulation and on-truck, as all that information is already available to the on-board prototype computer.

REFERENCES

REFERENCES

[1] Oak Ridge National Laboratory. Freight analysis framework version 4. https://faf.ornl.gov/faf4/Extraction1.aspx, 2019.

[2] Electric vehicle outlook. Technical report, BloombergNEF, 2019.

[3] Inventory of u.s. greenhouse gas emissions and sinks: 1990-2018. Technical report, United States Environmental Protection Agency, 2020.

[4] American Trucking Associations. Professional truck drivers and the trucking industry. https://www.trucking.org/sites/default/files/2019-12/pro/20Truck/20Drivers_final.pdf, 2018.

[5] EPA New England. Nitrogen oxides (nox) control regulations. https://www.epa.gov/air-emissions-inventories/2011-national-emissions-inventory-nei-data, 2011.

[6] A.I. Guerrero de la Peña. *Development of a framework for projecting line-haul truck technology adoption and greenhouse gas emissions in the U.S. using a System-of-Systems methodology*. PhD thesis, Purdue University - West Lafayette, 3 2020.

[7] Nitrogen oxides (nox), why and how they are controlled. Technical report, Clean Air Technology Center (MD-12), Information Transfer and Program Integration Division, Office of Air Quality Planning and Standards, U.S. Environmental Protection Agency, 1999.

[8] W. Barcikowski et al. Final 2016 air quality management plan. Technical report, South Coast Air Quality Management District, 2017.

[9] DieselNet Emission Standards. United states: Heavy-duty onroad engines. https://dieselnet.com/standards/us/hd.php, 2020.

[10] DieselNet Emission Standards. Heavy-duty ftp transient cycle. https://dieselnet.com/standards/cycles/ftp_trans.php, 2020.

[11] H. Jääskeläinen and W.A. Majewski. Heavy-duty diesel engines with aftertreatment. Technical report, DieselNet Technology Guide, 2018.

[12] W.A. Majewski. Selective catalytic reduction. Technical report, DieselNet Technology Guide, 2005.

[13] R. Sala, J. Krasowski, and J. Dzida. The influence of engine warm up phase on nitrogen oxides emission for heavy-duty euro vi diesel engine. In *International Congress on Combustion Engines*. MATEC Web of Conferences, 2017.

[14] H. Jääskeläinen and W.A. Majewski. Engine emission control. Technical report, DieselNet Technology Guide, 2019.

[15] California air resources board staff current assessment of the technical feasibility of lower nox standards and associated test procedures for 2022 and subsequent model year medium-duty and heavy-duty diesel engines. Technical report, California Air Resource Board, Mobile Source Control Division, Mobile Source Regulatory Development Branch, 2019.

[16] National Research Council. *Vehicle Technologies for Reducing Load-Specific Fuel Consumption*, pages 91–92. The National Academies Press, 2010.

[17] A. Ragatz and M. Thornton. Aerodynamic drag reduction technologies testing of heavy-duty vocational vehicles and a dry van trailer. Technical report, National Renewable Energy Laboratory, Golden, CO, 2016.

[18] R.M. Clarke. Test, evaluation, and demonstration of practical devices/systems to reduce aerodynamic drag of tractor/semitrailer combination unit trucks. Technical report, Truck Manufacturers Association, Morgantown, WV, 2007.

[19] J. Hawkins. Trailer aerodynamic device combination testing: On-road and coast-down. In *SAE COMVEC*. SAE International, 2018.

[20] J. Smith. High yaw angle vehicle drag reduction utilizing affirimative aerodynamic propulsive elements. In *SAE COMVEC*. SAE International, 2018.

[21] Peloton Technology. The platooning experience. `https://peloton-tech.com/how-it-works/`, 2020.

[22] M. Lammert, K. Kelly, and J. Yanowitz. Correlations of platooning track test and wind tunnel data. Technical report, National Renewable Energy Laboratory, Golden, CO, 2018.

[23] Electronic drawbar - digital innovation project report - presentation of the results. Technical report, MAN Truck and Bus, DB Schenker and the Hochschule Fresenius, 2019.

[24] M.P. Lammert, A. Duran, J. Diez, K. Burton, and A. Nicholson. Effect of platooning on fuel consumption of class 8 vehicles over a range of speeds, following distances, and mass. *SAE Int. J. Commer. Veh*, 7:626–639, 2014.

[25] M.P. Lammert, B. Bugbee, Y. Hou, A. Mack, M. Muratori, J. Holden, A. Duran, and E. Swaney. Exploring telematics big data for truck platooning opportunities. In *SAE World Congress Experience*. SAE International, 2018.

[26] D. Chena, S. Ahnb, M. Chitturib, and D. Noyce. Truck platooning on uphill grades under cooperative adaptive cruise control (cacc). *Transportation Research Procedia*, 23:50–66, 2017.

[27] A. Alam, B. Besselink, V. Turri, J. Mårtensson, and K.H. Johansson. Heavy-duty vehicle platooning for sustainable freight transportation. *IEEE Control Systems Magazine*, pages 34–56, 2015.

[28] D. Culbertson, M. Khair, S. Zhang, J. Tan, and J. Spooler. The study of exhaust heating to improve scr cold start performance. *SAE International Journal of Engines*, 8:1187–1195, 2015.

[29] M. Kimura, T. Muramatsu, E. Kunishima, J. Namima, W. Crawley, and T. Parrish. Development of the burner systems for epa2010 medium duty diesel vehicles. In *SAE 2011 World Congress*. SAE International, 2011.

[30] H. Kojima, M. Fischer, H. Haga, N. Ohya, K. Nishi, T. Mito, and N. Fukushi. Next generation all in one close-coupled urea-scr system. In *SAE 2015 World Congress*. SAE International, 2015.

[31] K.R. Vos, G.M. Shaver, M.C. Joshi, and Jr J. McCarthy. Implementing variable valve actuation on a diesel engine at high-speed idle operation for improved aftertreatment warm-up. *International Journal of Engine Research*, 2019.

[32] C.A. Sharp, C.C. Webb, Sr. G.D. Neely, and I. Smith. Evaluating technologies and methods to lower nitrogen oxide emissions from heavy-duty vehicles. Technical report, Southwest Research Institute, San Antonio, TX, 2017.

[33] D.B. Gosala, A.K. Ramesh, C.M. Allen, M.C. Joshi, A.H. Taylor, M. Van Voorhis, G.M. Shaver, L. Farrell, E. Koeberlein, J. McCarthy Jr, and D. Stretch. Diesel engine aftertreatment warm-up through early exhaust valve opening and internal exhaust gas recirculation during idle operation. *International Journal of Engine Research*, 19:758–773, 2018.

[34] M.C. Joshi. *Opportunities to Improve Aftertreatment Thermal Management and Simplify the Air Handling Architectures of Highly Efficient Diesel Engines Incorporating Valvetrain Flexibility*. PhD thesis, Purdue University - West Lafayette, 1 2020.

[35] M.C. Joshi, D.B. Gosala, C.M. Allen, K. Vos, M. Van Voorhis, A. Taylor, G.M. Shaver, J. McCarthy Jr., D. Stretch, E. Koeberlein, and L. Farrell. Reducing diesel engine drive cycle fuel consumption through use of cylinder deactivation to maintain aftertreatment component temperature during idle and low load operating conditions. *Frontiers in Mechanical Engineering*, 3:8, 2017.

[36] I.J Ibitayo. Enhanced Class 8 Truck Platooning via Simultaneous Shifting and Model Predictive Control, 8 2019.

[37] A. Alam, J. Mårtensson, and K.H. Johansson. Look-ahead cruise control for heavy duty vehicle platooning. In *IEEE Annual Conference on Intelligent Transportation Systems*. IEEE, 2013.

[38] T.E. Odstrcil. Variable valve actuation strategies for improving aftertreatment system efficiency in modern diesel engines over the heavy-duty federal test procedure certification cycle, 2018.

[39] 2015 work truck electrification and idle management study: Study exploring advanced vehicle technologies. Technical report, National Truck Equipment Association, Farmington Hills, MI, 2015.

[40] C. Ding. *Thermal efficiency and emission analysis of advanced thermodynamic strategies in a multi-cylinder diesel engineutilizing valve-train flexibility*. PhD thesis, Purdue University - West Lafayette, 12 2014.

[41] D. Bevly, C. Murray, A. Lim, R. Turochy, R. Sesek, S. Smith, L. Humphreys, G. Apperson, J. Woodruff, S. Gao, M. Gordon, N. Smith, S. Praharaj, J. Batterson, R. Bishop, D. Murray, A. Korn, J. Switkes, S. Boyd, and B. Kahn. Heavy truck cooperative adaptive cruise control: Evaluation, testing, and stakeholder engagement for near term deployment: Phase two final report. Technical report, Auburn University, Auburn, AL, 2017.

[42] M. Ellis, J.I. Gargoloff, and R. Sengupta. Aerodynamic drag and engine cooling effects on class 8 trucks in platooning configurations. *SAE International Journal of Commercial Vehicles*, 8:732–739, 2015.

[43] J. Smith, R. Mihelic, B. Gifford, and M. Ellis. Aerodynamic impact of tractor-trailer in drafting configuration. *SAE International Journal of Commercial Vehicles*, 7:619–625, 2015.

[44] K. Salari and J. Ortega. Experimental investigation of the aerodynamic benefits of truck platooning. In *WCX World Congress Experience*. SAE International, 2018.